

# Sparse Representations of Positive Functions via Projected Pseudo-Mirror Descent

Abhishek Chakraborty, Ketan Rajawat, and Alec Koppel

## Abstract

We consider the problem of expected risk minimization when the population loss is strongly convex and the target domain of the decision variable is required to be nonnegative, motivated by the settings of maximum likelihood estimation (MLE) and trajectory optimization. We restrict focus to the case that the decision variable belongs to a nonparametric Reproducing Kernel Hilbert Space (RKHS). To solve it, we consider stochastic mirror descent that employs (i) *pseudo-gradients* and (ii) projections. Compressive projections are executed via kernel orthogonal matching pursuit (KOMP), and overcome the fact that the vanilla RKHS parameterization grows unbounded with time. Moreover, pseudo-gradients are needed, e.g., when stochastic gradients themselves define integrals over unknown quantities that must be evaluated numerically, as in estimating the intensity parameter of an inhomogeneous Poisson Process, and multi-class kernel logistic regression with latent multi-kernels. We establish tradeoffs between accuracy of convergence in mean and the projection budget parameter under constant step-size and compression budget for pseudo-gradients, as well as non-asymptotic bounds on the model complexity. Additionally we also show almost sure convergence to a small neighborhood of the optima for the stochastic gradients for the same constant parameter selection. Experiments demonstrate that we achieve state-of-the-art accuracy and complexity tradeoffs for inhomogeneous Poisson Process intensity estimation and multi-class kernel logistic regression.

## I. INTRODUCTION

Function fitting when the target domain is required to be nonnegative arises in numerous settings: trajectory optimization [1], [2], as well as unsupervised [3] and supervised learning [4] where the cost is given by a negative log-likelihood associated with a probabilistic model. In this work, we consider the nonnegative function estimation problems where the fitness criterion is a strongly convex cost that depends on sequentially observed samples from an unknown distribution, and the feasible set is a nonparametric function class called a reproducing kernel Hilbert Space (RKHS) [5]. Our specific technical contribution is a variant of pseudo-mirror descent that employs sparse subspaces projections, which yields a tunable tradeoff between convergence accuracy and function complexity. Our driving motivations are efficient representations of the intensity parameter of an inhomogeneous Poisson Process [6] and multi-class kernel logistic regressors [7].

Let us set aside the issue of nonnegativity and function representation for now, and consider the simpler problem of finding linear statistical models by solving an optimization problem over the Euclidean space. Then, the problem under consideration is simply a convex program, which, when analytical expressions are unavailable, may be solved effectively with Newton or gradient methods to global optimality [8]. Doing so hinges upon gradient information being efficiently computable, which breaks down when the cost is defined by an expectation over an unknown distribution, only realizations of which are available [9], as in *expected risk minimization*. For such settings, stochastic approximations are necessary [10], which use stochastic gradients (or stochastic Quasi-Newton updates) in lieu of exact updates. Their performance is then inherently tethered to the properties of the unknown data distribution, and one may guarantee their performance often only probabilistically [11]. In this work, we build upon a stochastic variant of proximal gradient method [12], i.e., stochastic mirror descent, which substitutes Euclidean distance by a Bregman divergence in its local update rule, which refines the convergence of first-order stochastic methods when the feasible set is structured [13], such as, e.g., the probability simplex [14].

The strong guarantees for Euclidean settings belies the fact that linear models are outperformed by universal function approximators [15]. Specifically, deep neural networks (DNNs) [16] and kernel methods [17] have set the standard across disparate domains: computer vision [18], natural language processing [19], [20], autonomous control [21], and a plethora of others. In this work, we focus on RKHS parameterizations due to the fact that (i) under suitable choice of kernel, they in fact may be shown to be equivalent to certain DNNs [22]; (ii) their training defines a convex program over a Hilbert space [23]; and (iii) one may directly co-design the choice of kernel and Bregman divergence for likelihood-based objectives [24].

One challenge associated with the RKHS setting is that the function's representational complexity, owing to the Representer Theorem [25], is proportional to the sample size, which for expected risk minimization, approaches infinity. A myriad of approaches to approximating functions belonging to RKHS exist: those based upon matrix factorization [26] and spectral properties of the kernel matrix [27], [28], random feature techniques that exploit the fact that the kernel defines a distribution over the feature space [29], from which one may employ random sampling [30], [31], and methods that employ subspace projections [32] based upon greedy compression [33]. Among kernel approximations, subspace projection methods that fix the

A. Chakraborty is currently affiliated to NetApp, India and he did this work as a part of his M.Tech thesis at IIT Kanpur {Email: chakrabortyabhishek1994@gmail.com}. K. Rajawat is with Dept. of EE, IIT Kanpur, India {Email: ketan@iitk.ac.in}. A. Koppel is with CISD, U.S. Army Research Laboratory, Adelphi, MD, USA {Email: alec.e.koppel.civ@mail.mil}.

per-update error rather than the complexity have been shown to obtain the strongest performance in theory and practice [34], [35], and hence we adopt them here to sparsify stochastic descent directions in RKHS.

We focus on a variant of the RKHS-function fitting problem when the function range is required to be nonnegative. Positivity is of interest in the problem of fitting the intensity parameter of inhomogeneous point processes (stochastic processes that count the number of events over a time increment) [36], supervised learning when the objective is associated with a negative log-likelihood [14], and trajectory optimization over Euclidean space [1], [2]. Two intertwined challenges emerge when addressing learning nonnegative functions: how to enforce the constraint, and whether the stochastic gradient is evaluable. Upon suitable initialization, one may ensure updates remain within the space of positive functions via selecting the Bregman divergence as the I-Divergence (or KL) [37]. However, the gradient may only be partially evaluable, due to, for instance, the need to numerically evaluate an integral [38], or the true kernel is a latent convolution of one’s chosen kernels [39]. In this case, *pseudo-gradients* [40], i.e., stochastic descent directions that are positively correlated with the true gradient, are the only update directions that are available. Moreover, their use in stochastic pseudo-mirror descent has recently achieved state of the art performance in intensity estimation in point processes [38]. In this work, we improve upon this approach by designing projected variants that yield tunable tradeoffs between convergence accuracy and complexity, and in doing so, set a new standard for performance in practice. More specifically, our technical contributions to:

- (i) formulate the expected risk minimization problem over RKHS functions with nonnegative range (Sec. II);
- (ii) develop mirror descent that uses pseudo-gradients in the RKHS setting (Sec. III), and put forth a compressive projection operator over the auxiliary gradient sequence of distance-like functions defined by the Bregman divergence. Together, we obtain specific parametric updates in terms of weights and past training examples;
- (iii) establish that the resulting algorithm converges linearly in expectation up to a bounded error neighborhood under constant step-size and compression parameter. Along with establishing the convergence results with pseudo-gradients, we also showed almost sure convergence results in the neighborhood of the optimum for the same parameter selection for stochastic gradients, which is a special case of pseudo-gradients. We further establish a non-asymptotic complexity characterization of the learned function’s parameterization (Sec. IV);
- (iv) evaluate numerically the proposed approach for two canonical examples: fitting the intensity parameter of an inhomogeneous Poisson Process on synthetic 1-D Gaussian toy dataset and real world NBA Stephen Curry dataset [38]; and multi-class kernel logistic regression on real life MNIST handwritten dataset [41] (Sec. V). In both instances, we observe a favorable tradeoff between model fitness, representational complexity, and interpretability of the resultant model relative to offline and online benchmarks.

**Notation** We denote functions by small scalar alphabets such as  $f$  and  $g$ . The Hilbert space is denoted by  $\mathcal{H}$  and its dual space by  $\mathcal{H}^*$ . All norms applied to elements of  $\mathcal{H}$  are Hilbert norms, henceforth denoted simply by  $\|\cdot\|$ . The norm applied on the elements of the  $\mathcal{H}^*$  are represented as  $\|\cdot\|_*$ .

## II. PROBLEM FORMULATION

Consider the problem of expected risk minimization in the online setting: independent identically distributed (i.i.d.) training samples  $\{\mathbf{x}_t\}_{t \geq 1}$  are observed in a sequential manner. Here,  $\mathbf{x}_t \in \mathcal{X} \subset \mathbb{R}^d$  denote the instances or input data points. In this work, we consider a formulation that is applicable to supervised and unsupervised learning, and develop specialized algorithms for both of them when the merit criterion is defined by a probabilistic mode, such as, e.g., logistic regression and Poisson Process intensity estimation.

**Supervised Learning.** Specifically, for supervised learning, target variables  $y_t \in \mathcal{Y}$  are also received corresponding to each  $\mathbf{x}_t$ , where  $y_t \in \mathcal{Y}$  denote the labels or real values, i.e.,  $\mathcal{Y} = \{1, \dots, C\}$  in the case of classification and  $\mathcal{Y} \subset \mathbb{R}$  in the case of regression. The examples  $(\mathbf{x}_t, y_t)$  are realizations from an unknown distribution  $\mathbb{P}(\mathbf{x}, y)$ . The goal is to fit a predictive model  $f : \mathcal{X} \rightarrow \mathcal{Y}$  that belongs to a particular hypothesized class of functions  $\mathcal{H}$ , i.e., to form estimates of the target of the form  $\hat{y}_t = f(\mathbf{x}_t)$ . The merit of a given estimator  $f$  is quantified by a convex loss  $\ell : \mathcal{H} \times \mathcal{X} \rightarrow \mathcal{Y}$  which is small when  $f(\mathbf{x})$  and  $y$  are close  $\ell(f(\mathbf{x}), y)$ , which we seek to minimize in expectation over data through the statistical loss  $R(f) := \mathbb{E}[\ell(f(\mathbf{x}), y)]$ . Example include the squared loss  $(y - f(\mathbf{x}))^2$ , the hinge loss  $\max\{0, 1 - yf(\mathbf{x})\}$ , and the logistic loss derived from minimizing the class-conditional misclassification probability – see [4].

**Unsupervised Learning.** For unsupervised learning, i.e., generative modeling, only realizations  $\mathbf{x}_t$  from a fixed unknown distribution  $\mathbb{P}(\mathbf{x})$  are received. The goal is to fit a (possibly unnormalized) density  $f$  that belongs to the hypothesis space  $\mathcal{H}$ . The particular target domain is defined by a likelihood model, which induces a loss function  $\ell(f(\mathbf{x}))$ , typically defined as the negative log-likelihood of a probabilistic (generative) model, which we seek to minimize in expectation over the unknown data distribution  $\mathbb{P}(\mathbf{x})$ , i.e.,  $R(f) := \mathbb{E}[\ell(f(\mathbf{x}))]$ .

Both settings may be subsumed into the stochastic program

$$f^* = \arg \min_{f \in \mathcal{H}_+} R(f) \quad (1)$$

where  $R(f)$  is  $\lambda$ -strongly convex. Henceforth, to unify notation, we write the instantaneous costs as  $r_t(f) := \ell(f(\mathbf{x}_t), y_t)$  and  $r_t(f) := \ell(f(\mathbf{x}_t))$  respectively corresponding to the data point pair  $\mathbf{x}_t, y_t$  for first case and data point  $\mathbf{x}_t$  for second case

respectively. We focus on the case that the range of  $f$  is nonnegative, which belongs to function class denoted as  $\mathcal{H}_+$ . This setting arises inherently in the estimation of probabilistic models and intensity estimation that arises in point processes.

Before continuing, we clarify the function class  $\mathcal{H} \supset \mathcal{H}_+$  to which estimators  $f$  belong. Specifically, we hypothesize that  $\mathcal{H}$  is a Hilbert space associated with symmetric positive definite kernel  $\kappa$  that satisfies  $\mathcal{H} := \text{span}(\kappa(\mathbf{x}, \cdot))$ , where every  $f \in \mathcal{H}$  can be written as linear combination of the kernel evaluations. The elements of  $\mathcal{H}$  also satisfy the reproducing property which states that  $\langle f, \kappa(\mathbf{x}, \cdot) \rangle = f(\mathbf{x})$  for all  $\mathbf{x} \in \mathcal{X}$ . Hilbert spaces of this type are called reproducing kernel Hilbert spaces (RKHS). Examples range from simple kernel functions such as the Gaussian kernel  $\kappa(\mathbf{x}, \mathbf{x}') = \exp(-\|\mathbf{x} - \mathbf{x}'\|^2/2c)$  and polynomial kernel  $\kappa(\mathbf{x}, \mathbf{x}') = (\mathbf{x}^\top \mathbf{x}' + b)^c$ , to sophisticated data-dependent convolutional kernels [39].

With the problem setting and the function class over which we search made clear, we present two representative examples: Poisson intensity estimation and kernel logistic regression.

**Example 1. Poisson Point Process intensity estimation:** Poisson Processes are a family of probabilistic models used to model the count of events  $N(\mathcal{T})$  within an interval  $\mathcal{T} \subset \mathcal{S} \subset \mathbb{R}^d$ .  $N(\cdot)$  is a stochastic process that counts the number of points up to its argument which belongs to set  $\mathcal{T}$ . A fundamental question that arises in its use is the intensity parameter  $\lambda(\cdot)$ , which determines the rate  $\lambda(s)$  at which new events occur in an infinitesimally small time-increment, i.e.,  $\lambda(s) = \lim_{\Delta s \rightarrow 0} \mathbb{E}[N(\Delta s)]/(\Delta s)$ . In inhomogeneous cases, this parameter is a nonlinear function, such that the likelihood associated with Poisson points  $\{\mathbf{t}_n\}_{n=1}^N$  takes the form:

$$L(f) = \prod_{n=1}^N \lambda(\mathbf{t}_n) \exp \left\{ - \int_{\mathcal{S}} \lambda(\mathbf{t}) dt \right\} \quad (2)$$

Then, one may construct an instantiation of (1) by considering the negative log-likelihood of (2), inspired by [42]:

$$R(f) = - \sum_{n=1}^N \log(\lambda(\mathbf{t}_n)) + \int_{\mathcal{S}} \lambda(\mathbf{t}) dt \quad (3)$$

where one may identify that the Poisson points  $\mathbf{t}_n$  play the role of  $\mathbf{x}_n$ , and  $\lambda(\cdot)$  is the known function  $f(\cdot)$  we seek to estimate – note that  $\lambda(\cdot)$  is required to be nonnegative. This is an instance of unsupervised learning which has been studied both when  $\{\mathbf{t}_n\}_{n=1}^N$  are available all at once or revealed incrementally, respectively, in [42] and [38]. Here we develop online approaches to memory-efficient solutions to (3). Further derivation details may be found in [3]

**Example 2. Logistic regression for multi-class classification:** In this case, the target domain  $\mathcal{Y} = \{1, \dots, C\}$  is the set of classes, and the loss is defined by the negative log-likelihood of a generalized odds ratio. Specifically, define a vector-function associated with a one-hot encoding, i.e., the target domain is  $\{0, 1\}^C$ , such that each  $\mathbf{x}$  is assigned to a binary vector of length  $C$ . Then, one hypothesizes that the probability of the predicted label  $y$  to lie in the class  $c$  is given by the logit (softmax) function  $\mathbb{P}(y = c | \mathbf{x}) := \frac{\exp(f_c(\mathbf{x}))}{\sum_{\tilde{c}} f_{\tilde{c}}(\mathbf{x})}$ , which gives rise to the negative log-likelihood: [4]

$$\ell(\mathbf{f}, \mathbf{x}_t, y_t) = - \log(\mathbb{P}(y = y_t | \mathbf{x}_t)) \quad (4)$$

$$= \log \left( \sum_{\tilde{c}} f_{\tilde{c}}(\mathbf{x}_t) \right) - f_{y_t}(\mathbf{x}_t) \quad (5)$$

where  $\mathbf{f}$  denotes vector of functions  $f_{\tilde{c}}$  where  $\tilde{c}$  denotes each of the class labels, and the classification of a point  $\mathbf{x}$  is defined by the maximum a posteriori assignment:  $\hat{c} = \arg \max_{c \in \{1, \dots, C\}} f_c(\mathbf{x})$ . Observe that the space of binary sequences  $\{0, 1\}^C$  is nonnegative, meaning that minimizing (5) in expectation over  $\mathbb{P}(\mathbf{x}, y)$  is an instance of (1).

In this work, we focus on algorithms to solve (1) by designing search directions that allow the function to move in the interior of the (generalized) probability simplex. Before doing so, we close the section with a clarifying remark about the complexity implications of searching over RKHS.

**Remark 1. (Empirical Risk Minimization)** An important special case of (1) is *empirical risk minimization* (ERM) where a fixed collection of data ( $\mathcal{D} := \{(\mathbf{x}_i, y_i)_{i=1}^N\}$  for supervised and  $\mathcal{D} := \{\mathbf{x}_i_{i=1}^N\}$  for unsupervised) is available, and we seek to find the empirical predictor

$$\hat{f}_N = \arg \min_{f \in \mathcal{H}} \frac{1}{N} \sum_{i=1}^N r_i(f) \quad (6)$$

Observe that  $\hat{f}_N$  in (6) is belongs to a Hilbert space, and hence is infinite-dimensional. However, the Representer Theorem, [43], [44] establishes that  $\hat{f}_N$  takes the form:

$$\hat{f}_N(\cdot) = \sum_{i=1}^N w_i \kappa(\mathbf{x}_i, \cdot) \quad (7)$$

where  $\{w_m\}_{m=1}^N$  are some real-valued weights. Substituting (7) into (6) reduces search over  $\mathcal{H}$  to real-valued space  $\mathbb{R}^N$ :

$$\hat{\mathbf{w}}_N = \arg \min_{\mathbf{w} \in \mathbb{R}^N} \frac{1}{N} \sum_{i=1}^N r_i(\mathbf{w}^\top \mathbf{k}_{\mathcal{D}}(\mathbf{x}_i)), \quad (8)$$

where we have collected kernel evaluations  $\{\kappa(\mathbf{x}_i, \mathbf{x}_j)\}_i$  into a vector called the empirical kernel map  $\mathbf{k}_{\mathcal{D}}(\mathbf{x}_i) \in \mathbb{R}^N$  and  $\{\kappa(\mathbf{x}_i, \mathbf{x}_j)\}_{i,j}$  into the Gram, or kernel, matrix  $\mathbf{K}_{\mathcal{D}\mathcal{D}} \in \mathbb{R}^{N \times N}$ . Observe that as the sample size  $N \rightarrow \infty$ , due to the curse of kernelization, it is not enough to solve (1) to optimality, but one must do so while also ensuring that the memory complexity remains bounded.

### III. ALGORITHM FORMULATION

Now we shift focus to deriving an iterative approach to solving (1) via a functional extension of mirror descent [45]. We select a Bregman divergence that ensures positivity of the range of the function  $f$  during optimization, and present a generalization of a gradient called a ‘‘pseudo-gradient’’ [40]. The merit of employing pseudo-gradients is the ability to define approximate search directions that are useful in integral approximations that arise in point process intensity estimation, as well as a broader ability to incorporate samples into the functional representation through a kernel embedding.

**Bregman Divergence** We proceed by presenting technicalities pertaining to the mirror map and the Bregman divergence before defining the variants of the proposed algorithm. Let  $\psi : \mathcal{H} \rightarrow \mathbb{R}$  be a proper, closed, smooth, and strongly convex functional. The Fenchel conjugate of  $\psi$  is denoted as  $\psi^* : \mathcal{H}^* \rightarrow \mathbb{R}$ , where  $\mathcal{H}^*$  is the dual space of  $\mathcal{H}$ . Define the shorthand for the objective evaluated at the gradient of the dual  $R_\psi(z) = (R \circ \nabla \psi^*)(z) = R(\nabla \psi^*(z))$  where  $z \in \mathcal{H}^*$ . This composition allows one to write  $\nabla R_\psi(\nabla \psi(f)) = \nabla R(f)$ ,  $f \in \mathcal{H}$  since  $\nabla \psi^* = (\nabla \psi)^{-1}$ . This identity will be employed later in the convergence analysis. The purpose of defining functional  $\psi$  is that it induces a distance-like functional Bregman divergence  $B_\psi : \mathcal{H} \times \mathcal{H} \Rightarrow \mathbb{R}$  [46]:

$$B_\psi(f, \tilde{f}) := \psi(f) - \psi(\tilde{f}) - \langle \nabla \psi(\tilde{f}), f - \tilde{f} \rangle_{\mathcal{H}}. \quad (9)$$

The functional Bregman divergence in (9) satisfies most of the properties of the vector Bregman divergence, including non-negativity, strong-convexity in the first argument, as well as a generalized Pythagorean theorem. Next we present a few examples – see [46].

- i) *Squared difference*: The choice  $\psi(f) = \frac{1}{2} \|f\|^2$  leads to the canonical case of  $B_\psi(f, \tilde{f}) = \frac{1}{2} \|f - \tilde{f}\|^2$ .
- ii) *Squared Mahalanobis difference*: Let  $\mathcal{L}$  be a compact self-adjoint operator, then the choice  $\psi(f) = \frac{1}{2} \langle \mathcal{L}f, f \rangle_{\mathcal{H}}$  results in the Bregman divergence  $B_\psi(f, \tilde{f}) = \frac{1}{2} \langle \mathcal{L}(f - \tilde{f}), f - \tilde{f} \rangle_{\mathcal{H}}$ , which generalizes the squared difference. For the simple case when  $\mathcal{L}$  is a diagonal operator, it amounts to pointwise multiplication with a weight function.
- iii) *KL-divergence or I-divergence*: Let  $\mathcal{H}$  be the space of probability density functions, constructed from a radial kernel such as Gaussian, Student-t, or Laplacian [47]. When, define  $\psi(f) = \langle f, \log(f) - 1 \rangle_{\mathcal{H}}$  similar to [38] yields  $B_\psi(f, \tilde{f}) = \langle f, \log(f/\tilde{f}) \rangle_{\mathcal{H}}$  if  $f$  is absolutely continuous with respect to  $\tilde{f}$  and is a probability density so that its total probability sums to 1. For this case,  $B_\psi$  is the KL-divergence or I-divergence associated with the convex map  $\psi(f) = \langle f, \log(f) - 1 \rangle_{\mathcal{H}}$  [37].

**Pseudo-Gradient** With Bregman divergence clarified, we shift to defining pseudo-gradients, which are those directions  $g_t$  with nonnegative expected (unnormalized) cosine similarity with the gradient  $\nabla_f R(f)$ :

$$\langle \nabla R(f_t), \mathbb{E}[g_t | \mathcal{F}_t] \rangle \geq 0 \quad (10)$$

where  $g_t$  is the pseudo gradient at  $t$ -th iteration and  $\mathcal{F}_t$  denotes the past sigma algebra which contains all the past data points one iteration back, i.e.  $\{\mathbf{x}_i\}_{i=1}^{t-1}$  or  $\{\mathbf{x}_i, y_i\}_{i=1}^{t-1}$  as the case maybe. Equivalently, a pseudo-gradient  $g_t$  is any search direction that forms an acute angle with the original gradient  $\nabla R(f_t)$  in the dual space, as stated in [40], and may be used in lieu of the true gradient when its evaluation is costly or intractable [38]. Next we present a few instances of pseudo-gradients to build intuition:

- i) *Stochastic Gradients*: If  $g_t$  is the stochastic gradient of  $R(\cdot)$  at  $f_t$ , then  $\mathbb{E}[g_t | \mathcal{F}_t] = \nabla R(f_t)$ . So the inner product  $\langle \nabla R(f_t), \mathbb{E}[g_t | \mathcal{F}_t] \rangle = \|\nabla R(f_t)\|_*^2 \geq 0$ .
- ii) *Kernel embedding*:  $\kappa : \mathcal{X} \times \mathcal{X} \rightarrow \mathbb{R}_+$  is a symmetric and positive definite kernel. So  $\langle G, \langle \kappa, G \rangle \rangle \geq 0$  for all vector  $G \in \mathcal{H}$ . Now  $g_t$  defined as  $g_t = \langle \kappa(\mathbf{x}_t, \cdot), \nabla R(f_t) \rangle$  is a pseudo-gradient since (10) is satisfied by the symmetric and positive definiteness property as given above.
- iii) *Gradient sign*: Define the gradient as  $g_t = \text{sgn}(\nabla R(f_t))$  where  $\text{sgn}$  denotes the sign operator. Then for all data points  $\mathbf{x} \in \mathcal{X}$ , the inner product of (10) is given as

$$\langle \nabla R(f_t), \text{sgn}(\nabla R(f_t)) \rangle = \int_{\mathcal{X}} |\nabla R(f_t(\mathbf{x}))| d\mathbf{x} \geq 0 \quad (11)$$

With these entities in hand, we define our approach to solving (1) online based upon streams of samples, which builds upon a functional variant of stochastic mirror descent:

$$f_{t+1} = \arg \min_{f \in \mathcal{H}} \left( \langle \nabla r_t(f_t), f \rangle_{\mathcal{H}} + \frac{1}{\eta_t} B_{\psi}(f, f_t) \right). \quad (12)$$

where  $\eta_t > 0$  is a nonnegative step-size that may be constant or time-varying. Subsequently, we focus on constant step-size  $\eta_t = \eta$  algorithms. Note that  $B_{\psi}(f, \tilde{f}) = \frac{1}{2} \|f - \tilde{f}\|^2$  reduces (12) to functional SGD. Moreover, clearly in order for (12) to be implementable, we require closed-form expressions for Bregman divergence. Note that for the squared Mahalanobis distance, the update takes the form  $f_{t+1} = f_t - \eta \mathcal{L}^{-1} \nabla r_t(f_t)$ , where the inverse  $\mathcal{L}^{-1}$  must be computable in closed-form.

In this work, motivated by computational issues arising in point processes, we study the use of employing pseudo-gradients  $g_t$  in (12) in lieu of stochastic gradients  $\nabla r_t(f_t)$ , where the loss is evaluated at the function iterate  $f_t$  using samples  $((\mathbf{x}_t, y_t)$  for supervised and  $\mathbf{x}_t$  for unsupervised), which takes the form

$$\tilde{f}_{t+1} = \arg \min_{f \in \mathcal{H}} \left( \langle g_t, f \rangle_{\mathcal{H}} + \frac{1}{\eta} B_{\psi}(f, f_t) \right). \quad (13)$$

To clarify how (13) is executable in practice, suppose for the moment that true stochastic gradient, i.e.,

$$\nabla r_t(f_t) = \begin{cases} \ell'(f_t(\mathbf{x}_t), y_t) \kappa(\mathbf{x}_t, \cdot), & \text{for supervised learning} \\ \ell'(f_t(\mathbf{x}_t)) \kappa(\mathbf{x}_t, \cdot), & \text{for unsupervised learning} \end{cases} \quad (14)$$

is used in the mirror descent update [cf. (12)] instead of the pseudo-gradient, i.e.,  $g_t = \nabla r_t(f_t) = \ell'(f_t, \mathbf{x}_t) \kappa(\mathbf{x}_t, \cdot)$  for both supervised and unsupervised learning in order to maintain notational congruence. For this case, then, the first-order optimality condition for (13) may be written as

$$g_t + \frac{1}{\eta} \nabla_{\tilde{f}_{t+1}} B_{\psi}(\tilde{f}_{t+1}, f_t) = 0 \quad (15)$$

Noting the fact  $\nabla_{\tilde{f}_{t+1}} B_{\psi}(\tilde{f}_{t+1}, f_t) = \nabla \psi(\tilde{f}_{t+1}) - \nabla \psi(f_t)$ , (15) can be expressed as

$$g_t + \frac{1}{\eta} (\nabla \psi(\tilde{f}_{t+1}) - \nabla \psi(f_t)) = 0 \quad (16)$$

Define  $\tilde{z}_{t+1} = \nabla \psi(\tilde{f}_{t+1})$  and  $z_t = \nabla \psi(f_t)^1$ , which after rearranging (16), yields

$$\tilde{z}_{t+1} = z_t - \eta g_t \quad (17)$$

Observe that  $z_t = \nabla \psi(f_t)$ , which implies  $f_t = \nabla \psi^*(z_t)$ , where  $\psi^*$  is the Fenchel conjugate of  $\psi$  and  $\nabla \psi^* = (\nabla \psi)^{-1}$ . Hence the update (17) becomes

$$\tilde{z}_{t+1} = z_t - \eta \ell'(\nabla \psi^*(z_t), \mathbf{x}_t) \kappa(\mathbf{x}_t, \cdot) \quad (18)$$

where (18) is derived via applying the chain rule and the reproducing property of the kernel to  $\nabla r_t(\nabla \psi^*(z_t))$  analogous to (14). Thus, the functional update is executable parametrically via a data set  $\mathcal{D}_{z,t}$  consisting of  $t - 1$  points that grows by one per time step with an associated coefficient vector  $\mathbf{w}_{z,t}$ :

$$\mathcal{D}_{z,t+1} = \mathcal{D}_{z,t} \cup \{\mathbf{x}_t\}, [\mathbf{w}_{z,t+1}]_n = \begin{cases} [\mathbf{w}_{z,t}]_n & \mathbf{x}_n \in \mathcal{D}_t \\ -\eta \ell'(\nabla \psi^*(z_t), \mathbf{x}_t) & \mathbf{x}_n = \mathbf{x}_t \end{cases} \quad (19)$$

where  $[\mathbf{w}_{z,t}]_n$  denotes the  $n$ -th coordinate of the vector  $\mathbf{w}_{z,t}$ .

We note that the function evaluation  $f$  at point  $\mathbf{x} \in \mathcal{X}$  then takes the form at time  $t + 1$

$$f_{t+1}(\mathbf{x}) = \nabla \psi^*(z_{t+1}(\mathbf{x})) = \nabla \psi^*(\mathbf{w}_{z,t+1}^{\top} \mathbf{k}_{\mathcal{D}_{z,t+1}}(\mathbf{x})) \quad (20)$$

These derivations do not carry through to the general pseudo-gradient  $g_t \neq \nabla r_t(f_t)$  since (16) cannot be evaluated in closed form. However, for the case of the kernel embedding (ii) mentioned on the previous page, (19) takes the form

$$\mathcal{D}_{z,t+1} = \mathcal{D}_{z,t} \cup \{\mathbf{x}_t\}, [\mathbf{w}_{z,t+1}]_n = \begin{cases} [\mathbf{w}_{z,t}]_n & \mathbf{x}_n \in \mathcal{D}_t \\ -\eta g'_t & \mathbf{x}_n = \mathbf{x}_t \end{cases} \quad (21)$$

where the pseudo-gradient is assumed differentiable such that  $g_t = g'_t \kappa(\mathbf{x}_t, \cdot)$ . The kernel embedding, or any other pseudo-gradient, yields the specific form of  $g'_t$ .

Importantly, due to the RKHS parameterization in terms of weights and feature vectors  $\mathbf{x}_t$ , the complexity of the function grows unbounded with time  $t$ . We propose to ameliorating this issue with projections onto low-dimensional subspaces near

<sup>1</sup>Subsequently, we note that  $\{z_t\} \subset \mathcal{H}_*$ , i.e.,  $z_t$  is an element of the dual space  $\mathcal{H}_*$  of the RKHS  $\mathcal{H}$  defined at the outset of Sec. II.

---

**Algorithm 1** SPPPOT: Sparse Positive Functions via Projected Pseudo-Mirror Descent
 

---

**Require:** kernel  $\kappa$ , step-size  $\eta$ , compression parameter  $\epsilon$

- 1: **Initialize** Arbitrary small  $z_0$
- 2: **for**  $t = 1, 2, \dots$  **do**
- 3: **Read:** sample  $((\mathbf{x}_t, y_t)$  for supervised;  $\mathbf{x}_t$  for unsupervised)
- 4: **Evaluate:** Pseudo Gradient  $g_t$
- 5: **Update:**  $\tilde{z}_{t+1}$  as per (17)
- 6: **Compress:**  $\{\mathcal{D}_{t+1}, \mathbf{w}_{t+1}\} = \text{KOMP}(\tilde{\mathcal{D}}_{t+1}, \tilde{\mathbf{w}}_{t+1}, \epsilon)$
- 7: **Broadcast:**  $z_{t+1}$
- 8: **end for**
- 9: **Evaluation of actual function  $f_{t+1}$  at  $\mathbf{x}$ :** As per (20)

---



---

**Algorithm 2** Destructive Kernel Orthogonal Matching Pursuit (KOMP)
 

---

**Require:**  $\tilde{z}$  in form of  $(\tilde{\mathcal{D}}, \tilde{\mathbf{w}})$ , budget  $\epsilon$

**Initialize:**  $z = \tilde{z}$  so that  $(\mathcal{D}, \mathbf{w}) = (\tilde{\mathcal{D}}, \tilde{\mathbf{w}})$

**while**  $\mathcal{D} \neq \emptyset$  **do**

**for**  $\mathbf{x}_j \in \mathcal{D}$  **do**

Evaluate  $\mathbf{w}_j^* = \arg \min_{\mathbf{w}} \gamma_j(\mathbf{w}) := \|\tilde{z} - \sum_{\mathbf{x}_n \in \mathcal{D} \setminus \{\mathbf{x}_j\}} w_n \kappa(\mathbf{x}_n, \cdot)\|_*$

**end for**

**if**  $\gamma_j(\mathbf{w}_j^*) > \epsilon$  for all  $\mathbf{x}_j \in \mathcal{D}$  **then**

**break**

**else**

Prune  $\mathcal{D} \leftarrow \mathcal{D} \setminus \{\mathbf{x}_{j^*}\}$  where  $j^* = \arg \min \gamma_j$

Update weights  $\mathbf{w} \leftarrow \mathbf{w}_{j^*}^*$

**end if**

**end while**

**return**  $z$ , such that  $\|z - \tilde{z}\|_* \leq \epsilon$

---

the current search direction, which may be greedily obtained with kernel orthogonal matching pursuit (KOMP) [33], [48]. KOMP operates by, given an input dictionary  $\tilde{\mathcal{D}}_{z,t+1}$  and weight vector  $\tilde{\mathbf{w}}_{z,t+1}$ , returning a lower-dimensional (compressed) dictionary and weights  $\{z_{t+1}, \mathcal{D}_{z,t+1}, \mathbf{w}_{z,t+1}\} = \text{KOMP}(\tilde{z}_{t+1}, \tilde{\mathcal{D}}_{z,t+1}, \tilde{\mathbf{w}}_{z,t+1}, \epsilon)$  that are  $\epsilon$ -away in the RKHS norm, where  $\epsilon$  denotes the compression budget. Overall, then, the algorithm we propose takes the form

$$\{z_{t+1}, \mathcal{D}_{z,t+1}, \mathbf{w}_{z,t+1}\} = \text{KOMP}(\tilde{z}_{t+1}, \tilde{\mathcal{D}}_{z,t+1}, \tilde{\mathbf{w}}_{z,t+1}, \epsilon) \quad (22)$$

where  $\tilde{z}_{t+1}$  defined in (17) employs general pseudo-gradients – the overall procedure is summarized in Algorithm 1. Note KOMP is used differently from [34]: the RKHS-norm approximation criterion is in terms of the dual sequence  $\{z_t\}$  (18) as summarized in Algorithm 2.

**Examples.** With the iterative scheme given as Algorithm 1, we shift to discussing its specific form when the Bregman divergence is the (i) squared difference and (ii) KL-divergence.

- i) *Squared RKHS-norm difference:* For this case, the quantities in (17) take the form  $\tilde{z}_{t+1} = \nabla \psi(\tilde{f}_{t+1}) = \tilde{f}_{t+1}$  and  $z_t = \nabla \psi(f_t) = f_t$ , which gives the update rule

$$\tilde{f}_{t+1} = f_t - \eta g_t. \quad (23)$$

where the dictionary stacks past points [cf. (19)], and coefficients are updated as

$$\tilde{\mathbf{w}}_{t+1} = [\mathbf{w}_t, \quad -\eta g_t]. \quad (24)$$

When combined with KOMP-based subspace projections, this update is identical to POLK [34] under the additional specification that the pseudo-gradient is the stochastic gradient  $g_t = \nabla r_t(f_t)$  [cf. (14)].

- ii) *KL-divergence or I-divergence:* In this instance, the update for the auxiliary variables  $\tilde{z}_{t+1}$  and  $z_t$  (17) have the explicit forms  $\tilde{z}_{t+1} = \log(\tilde{f}_{t+1})$  and  $z_t = \log(f_t)$ , which may be substituted into (17) to yield an expression for  $\tilde{f}_{t+1}$  as

$$\log(\tilde{f}_{t+1}) = \log(f_t) - \eta g_t \quad (25)$$

which, following exponentiation, permits us to write

$$\tilde{f}_{t+1} = f_t \exp(-\eta g_t). \quad (26)$$

Observe from (26) that the update for  $f_t$  is non-linear and hence a vanilla application of the Representer Theorem (7) is not possible. However, by focusing on the auxiliary sequences  $\tilde{z}_{t+1} = \log(\tilde{f}_{t+1})$  and  $z_t = \log(f_t)$ , (26) permits linearization of the form (17), and hence a parametric weight update and dictionary update with respect to the auxiliary function  $\tilde{z}_{t+1}$  akin to (19). Note that from (26), the function  $\tilde{f}_{t+1}$  can be expressed recursively as a product of functions from  $f_0$  to  $f_t$ . So if the initialization for  $f_0$  is taken to be positive, and the projections in (22) are onto the space of functions with nonnegative range, then the function positivity is ensured throughout training. This is salient for Poisson intensity estimation (Example 1), logistic regression (Example 2), and MLE more broadly.

A key observation from the case of KL-Divergence is that since the update for  $f$  does not yield a linear basis expansion, it cannot be computed through weighted combinations of kernel evaluations (7). However, it can be recovered through inverting the logarithmic transformation, i.e.,  $f_{t+1}(\cdot) = \exp(z_{t+1}(\cdot)) = \exp(\mathbf{w}_{z,t+1}^\top \mathbf{k}_{\mathcal{D}_{z,t+1}}(\cdot))$ . Consequently, as each new datum  $\mathbf{x}$  arrives, we can obtain its evaluation under  $f$  as  $f_{t+1}(\mathbf{x}) = \exp(\mathbf{w}_{z,t+1}^\top \mathbf{k}_{\mathcal{D}_{z,t+1}}(\mathbf{x}))$ . This underscores the importance of the auxiliary sequences  $z_t$ . Observe that this phenomenon holds more broadly for any Bregman divergence when its update is nonlinear in  $f$  but the gradient of the Fenchel dual  $\nabla\psi^*(f)$  of its inducing map  $\psi(f)$  is efficiently computable.

The main merit of selecting different Bregman divergences is that, for a given step-size selection, we may tighten the rate of convergence both in theory and in practice, as we demonstrate in later sections. Subsequently, we suppress dependence on auxiliary variable  $z$  for simplicity, i.e.,  $\mathbf{w}_{t+1} = \mathbf{w}_{z,t+1}$  and  $\mathcal{D}_{t+1} = \mathcal{D}_{z,t+1}$ . Next, we expand upon gradient expressions of Examples 1 and 2, variants of which are employed experimentally Sec. V.

1) *Poisson Point Process*: Observe that for (3), the instantaneous loss for function  $f_t$  takes the form

$$\ell(f_t(\mathbf{x}_t)) = -\log(f_t(\mathbf{x}_t)) + \int_{\mathcal{X}} f_t(\mathbf{x}) d\mathbf{x}. \quad (27)$$

When no special form of  $f_t$  is known for analytically, one must evaluate the integral numerically using, e.g., Bayesian quadrature or kernel smoothing. We adopt the later approach, inspired by [42]: the quantity  $\int_{\mathcal{X}} f_t(\mathbf{x}) d\mathbf{x}$  is approximated by  $h \sum_{j \in \mathcal{U}} f_t(\mathbf{u}_j)$ , where  $\mathbf{u}_j$  are uniform grid points over the sample space  $\mathcal{X}$  whose indices lie in set  $\mathcal{U}$  and  $h$  is the infinitesimally small uniform grid area, similar to Trapezoidal rule for discrete approximations of integrals. Then differentiating with respect to  $f_t$  yields the pseudo-gradient

$$g_t = -\frac{1}{f_t(\mathbf{x}_t)} \kappa(\mathbf{x}_t, \cdot) + h \sum_{j \in \mathcal{U}} \kappa(\mathbf{u}_j, \cdot). \quad (28)$$

This is a pseudo-gradient because the second term of (28) can be seen as an approximated version of the integral using kernel embedding. Note that for the KL divergence/I-divergence, the transformation  $f_t = \exp(z_t)$  yields the pseudo-gradient  $g_t$ :

$$g_t = -\frac{1}{\exp(z_t(\mathbf{x}_t))} \kappa(\mathbf{x}_t, \cdot) + h \sum_{j \in \mathcal{U}} \kappa(\mathbf{u}_j, \cdot). \quad (29)$$

The subtlety of grid points versus Poisson points causes slight differences in the updates relative to (19). Specifically, in (29), the point  $\mathbf{x}_t$  are samples from the unknown Poisson process, while the points  $\mathbf{u}_j$  are fixed grid points across updates. These components come together to specify Algorithm 1 as follows:

- Initialize the dictionary  $\tilde{\mathcal{D}}_1$  with uniform grid points  $\mathbf{u}_j$  for all  $j \in \mathcal{I}_j$  where  $\mathcal{I}_j$  contain the indices of  $\mathbf{u}_j$ , with corresponding weight vector elements as  $\tilde{\mathbf{w}}_{z,1,j} = -\eta h$ .
- Receive Poisson samples  $\mathbf{x}_t$ , compute the pseudo-gradient (29), and update dictionary  $\tilde{\mathcal{D}}_{t+1} = \mathcal{D}_t \cup \{\mathbf{x}_t\}$ . The corresponding weight update is

$$\tilde{w}_{z,t+1,n} = \begin{cases} w_{z,t,n} - \eta h & \{\mathbf{x}_n = \mathbf{u}_j\} \in \mathcal{D}_t \\ w_{z,t,n} & \{\mathbf{x}_n \neq \mathbf{u}_j\} \in \mathcal{D}_t \\ \frac{\eta}{\exp(z_t(\mathbf{x}_t))} & \mathbf{x}_n = \mathbf{x}_t. \end{cases} \quad (30)$$

KOMP is then applied to the dictionary  $\tilde{\mathcal{D}}_{t+1}$  and weights  $\tilde{\mathbf{w}}_{t+1}$  to yield  $\mathcal{D}_{t+1}$  and  $\mathbf{w}_{t+1}$ . Since grid points  $\{\mathbf{u}_j\}$  are required to approximate the integral in the pseudo-gradient, their presence in the dictionary is fixed. Therefore, our selection scheme discerns which Poisson samples  $\mathbf{x}_t$  and associated weights  $w_t$  are statistically significant for estimating the inhomogeneous intensity parameter  $f(\cdot) = \lambda(\cdot)$  as in Example 1 of Sec. II.

2) *Logistic regression for multi-class classification*: Consider the setting of multi-class classification using a probabilistic generalization of the odds ratio which defines the loss (5). We differentiate it with respect to each  $f_{\tilde{c}}$  to obtain the functional stochastic gradient for each class where  $\tilde{c} \in \{1, \dots, C\}$ . The gradient expression takes the form:

$$g_t = \begin{cases} \frac{\exp(f_{c'}(\mathbf{x}_t))}{\sum_{\tilde{c}} \exp(f_{\tilde{c}}(\mathbf{x}_t))} \kappa(\mathbf{x}_t, \cdot) & c' \neq y_t \\ \left( \frac{\exp(f_{y_t}(\mathbf{x}_t))}{\sum_{\tilde{c}} \exp(f_{\tilde{c}}(\mathbf{x}_t))} - 1 \right) \kappa(\mathbf{x}_t, \cdot) & c' = y_t \end{cases} \quad (31)$$

The parametric updates for the entire function vector  $\mathbf{f}$  are carried out via (31), which operates upon the basis of a stream of samples  $\{\mathbf{x}_t, y_t\}$  in tandem with subspace projections.

With these instantiations of Algorithm 1 spelled out, we are ready to study its convergence properties. Before doing so, we close the section with a remark about pseudo-dual averaging.

**Remark 2. (Pseudo-Dual Averaging)** Dual averaging (see [49]) is closely related to mirror descent. Here, we expand upon these connections. Specifically, dual averaging with pseudo-gradients in the functional RKHS setting takes the form

$$\tilde{h}_{t+1} = h_t + g_t \quad (32)$$

$$\begin{aligned} f_{t+1} &= \arg \min_{f \in \mathcal{H}} \left( \langle h_{t+1}, f \rangle_{\mathcal{H}} + \frac{1}{\eta} \psi(f) \right) \\ &= \nabla \psi^*(-\eta h_{t+1}) \end{aligned} \quad (33)$$

and then one may apply KOMP on  $\tilde{h}_{t+1}$  with budget parameter  $\epsilon$  in order to ensure an efficient RKHS parameterization in terms of weights and dictionary elements. Here,  $\psi^*$  denotes the conjugate of  $\psi$ . In order for (33) to be valid, one requires  $\nabla \psi^* : \mathcal{H}^* \rightarrow \mathcal{H}$  so that  $f_{t+1} \in \mathcal{H}$ . For the stochastic case (a special case of pseudo gradient), the update can be written recursively as

$$\tilde{h}_{t+1} = h_t + \nabla r_t(\nabla \psi^*(-\eta h_t)) = h_t - \eta \tilde{g}_t \quad (34)$$

where  $\tilde{g}_t := -\frac{1}{\eta} \nabla r_t(\nabla \psi^*(-\eta h_t))$ . To see the link between the (32)-(33) and Algorithm 1, multiply (32) by  $-\eta$  and use the second update equation to obtain

$$\nabla \psi(\tilde{f}_{t+1}) = \nabla \psi(f_t) - \eta g_t \quad (35)$$

where  $\tilde{f}_{t+1} := \nabla \psi^*(-\eta \tilde{h}_{t+1})$ . This means that under an additional hypothesis that the gradient of the Fenchel conjugate of  $\psi$  does not take the functions  $h_t$  outside the RKHS, update expressions for dual averaging in updating  $h_t$  exactly coincides with  $z_t$  in (17). This link provides alternative potential ways of approaching the convergence theory of Algorithm 1, which are the subject of future work.

#### IV. CONVERGENCE ANALYSIS

We shift focus to analyzing the convergence behavior of Algorithm 1 in terms of iteratively solving (1) when the compression budget  $\epsilon$  and the step-size parameter  $\eta$  are held constant. We first present some technical conditions which are standard for analyzing stochastic methods.

**Assumption 1.** *The inner product between the gradient and the expectation of the pseudo-gradient given the filtration  $\mathcal{F}_t = \sigma(\{\mathbf{x}_i\}_{i=1}^{t-1})$ , is nonnegative.*

$$\langle \nabla R(f_t), \mathbb{E}[g_t | \mathcal{F}_t] \rangle \geq 0 \quad (36)$$

Moreover, its product-moment is lower bounded by the second-moment of the gradient in the dual norm:

$$\mathbb{E}[\langle \nabla R(f_t), \mathbb{E}[g_t | \mathcal{F}_t] \rangle] \geq D \mathbb{E}[\|\nabla R(f_t)\|_*^2] \quad (37)$$

where  $D$  is a positive constant.

**Assumption 2.** *The optimizer of (1) is finite  $\|f^*\|^2 \leq B$ .*

**Assumption 3.** *The function  $R$  is  $\lambda$ -strongly convex.*

**Assumption 4.** *The function  $R_\psi(\cdot)$  which takes as inputs the dual functions  $z = \nabla \psi(f)$  is  $L_1$ -smooth.*

**Assumption 5.** *The total expectation of the instantaneous gradient  $g_t$  is upper bounded by*

$$\mathbb{E}[\|g_t\|_*^2] \leq \sigma^2 + c^2 \mathbb{E}[\langle \nabla R(f_t), \mathbb{E}[g_t | \mathcal{F}_t] \rangle] \quad (38)$$

for all  $f \in \mathcal{H}$ ,  $t \in \mathbb{N}$ , and some real constants  $\sigma$  and  $c$ .

Assumption 1 asserts that an acute angle exists between the pseudo gradient  $g_t$  and actual gradient  $\nabla R(f_t)$ , and this angle can be no worse than 90 degrees, where the constant  $D$  determines how correlated these gradients are in the worst-case, which is used to establish decrement-like relationships in (52). Assumption 2 is employed in (58) to ensure that  $R(f_0) - R(f^*)$  is finite. Assumption 3 implies that Polyak Lojasiewicz (PL) condition holds and is required to replace an objective decrement with an RKHS-norm difference to the optimal function  $f^*$  in (55). Assumption 4 is standard in the analysis of mirror descent and proximal methods [12], and is used in the Bregman ‘‘three-point inequality’’ (48). Moreover, Assumption 5 permits us to establish boundedness of projected pseudo-gradients (Lemma 1). Thus, we consider more general conditions than [23], [34], where the compactness of the feature space is required.



Next, we define the notion of a projected pseudo-gradient in order to facilitate the analysis of Algorithm 1. To do so, recall the definition of the pseudo-gradient (16), which comes from the first-order optimality condition of (13). Because KOMP applied to the auxiliary sequence  $\tilde{z}_{t+1}$  yields the function iterate  $z_{t+1}$ , we define the *projected* pseudo-gradient  $\hat{g}_t$  as

$$\hat{g}_t := \frac{1}{\eta}(z_t - z_{t+1}) = \frac{1}{\eta}(\nabla\psi(f_t) - \nabla\psi(f_{t+1})). \quad (39)$$

which simplifies the evolution of the projected iterates  $z_t$  (17):

$$z_{t+1} = z_t - \eta\hat{g}_t. \quad (40)$$

Next we define some operations employed in the analysis:  $\mathbb{E}$  denotes the total expectation taken with respect to the unknown joint distribution ( $P(\mathbf{x}, y)$  for supervised and  $P(\mathbf{x})$  for unsupervised learning), and  $\mathbb{E}[g|\mathcal{F}_t]$  denotes the expectation of  $g$  conditioned on the filtration  $\mathcal{F}_t$ . For brevity, we also define:

$$\Gamma_t := \mathbb{E}\|\nabla R(f_t)\|_*^2. \quad (41)$$

where  $f^*$  is defined in (1),  $B_\psi$  is given in (9), and  $\|\cdot\|_*$  denotes the RKHS dual-norm as defined in Sec. II.

We begin by bounding the error in the projected pseudo-gradient (39) w.r.t. its un-projected variant (16), which is critical to establishing a descent property of Algorithm 1

**Lemma 1.** The directional error of the projected pseudo-gradient (39) relative to the pseudo-gradient [cf. (16)] as quantified by the RKHS dual-norm is bounded by the ratio of the compression budget to the step-size  $\epsilon/\eta$ . Moreover, it has bounded second-moment in the dual-norm:

$$\|\hat{g}_t - g_t\|_* \leq \frac{\epsilon}{\eta} \quad (42)$$

$$\mathbb{E}\|\hat{g}_t\|_*^2 \leq 2 \left( \left( \frac{\epsilon}{\eta} \right)^2 + \sigma^2 + c^2 \mathbb{E}[\langle \nabla R(f_t), \mathbb{E}[g_t|\mathcal{F}_t] \rangle] \right) \quad (43)$$

*Proof:* First, consider the dual-norm difference and substitute in the definitions of  $\hat{g}_t$  and  $g_t$  from (39) and (17) respectively, to obtain

$$\|\hat{g}_t - g_t\|_* = \frac{1}{\eta} \|z_{t+1} - \tilde{z}_{t+1}\|_* \leq \frac{\epsilon}{\eta} \quad (44)$$

which uses the fact that  $\nabla\psi(f_{t+1}) = z_{t+1}$  and  $\nabla\psi(\tilde{f}_{t+1}) = \tilde{z}_{t+1}$ . The KOMP stopping criterion  $\|z_{t+1} - \tilde{z}_{t+1}\|_* \leq \epsilon$  then yields (42). To obtain the second expression, consider  $\mathbb{E}\|\hat{g}_t\|_*^2$ , and add and subtract  $g_t$  inside the expectation to write

$$\begin{aligned} \mathbb{E}\|\hat{g}_t\|_*^2 &\leq 2\mathbb{E}\|g_t\|_*^2 + 2\mathbb{E}\|\hat{g}_t - g_t\|_*^2 \\ &\leq 2(\sigma^2 + c^2 \mathbb{E}[\langle \nabla R(f_t), \mathbb{E}[g_t|\mathcal{F}_t] \rangle]) + 2\mathbb{E}\|\hat{g}_t - g_t\|_*^2 \end{aligned} \quad (45)$$

where we use (38) via Assumption 5. ■

With this lemma established, we establish the mean convergence of Algorithm 1 under parameter selections.

**Theorem 1.** Under Assumptions 1-5, upon running Algorithm 1 for  $t + 1$  iterations, the objective sub-optimality attenuates linearly up to a bounded neighborhood when run with constant step-size  $\eta < \min(\frac{1}{q_1}, \frac{q_1}{q_2})$  and compression budget  $\epsilon = \alpha\eta$ ,

$$\mathbb{E}[R(f_{t+1}) - R(f^*)] \leq (1 - \rho)^t \mathbb{E}[R(f_0) - R(f^*)] + \frac{1}{\rho} \left[ L_1 \eta^2 \sigma^2 + \left( \frac{\eta \omega_1}{2} + L_1 \eta^2 \right) \alpha^2 \right] \quad (46)$$

Moreover, the function sub-optimality satisfies:

$$\mathbb{E}[\|f_{t+1} - f^*\|^2] \leq \frac{2}{\lambda} (1 - \rho)^t \mathbb{E}[R(f_0) - R(f^*)] + \frac{2}{\lambda \rho} \left[ L_1 \eta^2 \sigma^2 + \left( \frac{\eta \omega_1}{2} + L_1 \eta^2 \right) \alpha^2 \right] \quad (47)$$

where  $\rho = q_1 \eta - q_2 \eta^2$  with  $q_1 = 2\lambda \left( D - \frac{1}{2\omega_1} \right)$  and  $q_2 = 2\lambda D L_1 c^2$ ,  $D$  are positive constants:  $D$  is the correlation constant in Assumption 1,  $\omega_1$  is a constant of Peter-Paul's inequality such that  $\omega_1 > \frac{1}{2D}$ ,  $\alpha$  is the parsimony constant,  $\lambda > 0$  is the regularization parameter, and positive constant  $c^2$  coming from Assumption 5.

Theorem 1 characterizes the trade-off between the rate of the convergence and the radius of the ball to which the iterates converge at steady state. First note that regardless of the choice of  $\eta$  and  $t$ , the mean distance from the optimum will always be  $\mathcal{O}(\alpha^2)$  in the worst case. The bound in (47) is for  $\epsilon > 0$ , which causes the additional  $\alpha^2$  to appear. For  $\epsilon = 0$ , the  $\alpha^2$  term of (47) vanishes and hence simplifies to  $\frac{2}{\lambda \rho} \mathcal{O}(\eta^2 \sigma^2) = \mathcal{O}(\eta \sigma^2)$  asymptotically since  $\rho$  is approximately of order  $\eta$  for  $\eta < 1$ .

Further observe that the second term on the right-hand side of (46) and (47) simplifies to  $\mathcal{O}(\eta \sigma^2 + (1 + \eta) \alpha^2)$ . This means that the limiting distance from the optimum of the norm error decreases as  $\mathcal{O}(\eta + \alpha)$  by computing the square root of the expression in (47). These results are in accordance with the convergence rates of the iterates of stochastic mirror descent for

vector-valued problems [13], [50]. Theorem 1 is a generalization to the RKHS setting, where we additionally require the range of functions to be nonnegative. Moreover, we explicitly characterize the error in the convergence behavior incurred due to subspace projections of the auxiliary sequence  $z_t$  [cf. (22)]. Relative to [38][Theorem 6], our convergence result holds under comparable conditions, but incorporates the additional aspect of the parameterization efficiency/radius/rate of convergence tradeoffs associated with sparse projections. Specifically, for  $\epsilon = 0$  our result simplifies to the aforementioned result, but requires an RKHS parameterization that grows unbounded with the time index  $t$  due to (21).

*Proof of Theorem 1:* Recall the definition of  $R_\psi$  for the convex function  $\psi$  defined by Bregman divergence (9), i.e.,  $R_\psi(z) = (R \circ \nabla\psi^*)(z) = R(\nabla\psi^*(z))$  for  $z \in \mathcal{H}_*$ . Consider this quantity evaluated at auxiliary functions  $z_{t+1} = \nabla\psi(f_{t+1})$  and  $z_t = \nabla\psi(f_t)$ , and apply Assumption 4 regarding its Lipschitz continuity:

$$R_\psi(\nabla\psi(f_{t+1})) - R_\psi(\nabla\psi(f_t)) - \langle \nabla R_\psi(\nabla\psi(f_t)), \nabla\psi(f_{t+1}) - \nabla\psi(f_t) \rangle \leq \frac{L_1}{2} \|\nabla\psi(f_{t+1}) - \nabla\psi(f_t)\|_*^2. \quad (48)$$

Now, consider the expression for the projected pseudo-gradient in (39), which may be rearranged to obtain  $\nabla\psi(f_{t+1}) - \nabla\psi(f_t) = -\eta\hat{g}_t$ . Taken together with the fact that the dual of the Fenchel dual is the original function  $R(f_t) = R_\psi(\nabla\psi(f_t))$  one may rewrite (48) as an approximate descent relation as

$$\begin{aligned} R(f_{t+1}) &\leq R(f_t) - \langle \nabla R(f_t), \eta\hat{g}_t \rangle + \frac{L_1\eta^2}{2} \|\hat{g}_t\|_*^2 \\ &= R(f_t) - \eta\langle \nabla R(f_t), g_t \rangle + \eta\langle \nabla R(f_t), g_t - \hat{g}_t \rangle + \frac{L_1\eta^2}{2} \|\hat{g}_t\|_*^2. \end{aligned} \quad (49)$$

The right-hand side of this expression decomposes into four terms: (i) the objective at the previous step, (ii) the product-moment between the gradient and the pseudo-gradient, (iii) the directional error associated with pseudo-gradient projections, (iv) a second-moment of the projected pseudo-gradient in the RKHS dual norm. We proceed by concentrating on the third term of the right-hand side of (49). Via Peter-Paul's inequality and the KOMP stopping criteria (42), its expected value is upper-estimated as

$$\eta\mathbb{E}[\langle \nabla R(f_t), g_t - \hat{g}_t \rangle] \leq \frac{\eta}{2\omega_1} \Gamma_t + \frac{\eta\omega_1}{2} \left(\frac{\epsilon}{\eta}\right)^2, \quad (50)$$

where  $\omega_1$  is the Peter-Paul's inequality constant. Next we shift focus to the fourth term of the right-hand side of (49) whose expected value can be bounded as (43). So using (50) and (43), the total expectation of (49) becomes

$$\mathbb{E}[R(f_{t+1})] \leq \mathbb{E}[R(f_t)] - (\eta - L_1c^2\eta^2)\mathbb{E}[\langle \nabla R(f_t), \mathbb{E}[g_t|\mathcal{F}_t] \rangle] + \frac{\eta}{2\omega_1} \Gamma_t + \left(\frac{\eta\omega_1}{2} + L_1\eta^2\right) \left(\frac{\epsilon}{\eta}\right)^2 + L_1\eta^2\sigma^2. \quad (51)$$

So now, we concentrate on the second term of the right hand side of (51), whose expectation conditional on filtration  $\mathcal{F}_t$ , followed by total expectation is given as

$$-(\eta - c^2L_1\eta^2)\mathbb{E}[\langle \nabla R(f_t), \mathbb{E}[g_t|\mathcal{F}_t] \rangle] \leq -D(\eta - L_1c^2\eta^2)\Gamma_t, \quad (52)$$

where we have used Assumption 1, and the short-hand notation (41) for  $\Gamma_t$ . Now let's return focus to (51). Proceed by subtracting  $\mathbb{E}[R(f^*)]$  from both sides, and then substitute in the expression of (52) to formulate the relationship for the expected decrement  $\mathbb{E}[R(f_{t+1}) - R(f^*)]$ :

$$\mathbb{E}[R(f_{t+1}) - R(f^*)] \leq \mathbb{E}[R(f_t) - R(f^*)] - \left(D\eta - \frac{\eta}{2\omega_1} - DL_1c^2\eta^2\right)\Gamma_t + \left(\frac{\eta\omega_1}{2} + L_1\eta^2\right)\alpha^2 + L_1\eta^2\sigma^2, \quad (53)$$

where we have substituted in the choice of compression budget  $\epsilon = \alpha\eta$  for some scalar  $\alpha > 0$  in order to simplify fractions of the compression budget to the step-size that appear in the preceding expressions. Now we can apply strong convexity of the instantaneous (and hence population) objective as stated in Assumption 3 to write the PL condition

$$\|\nabla R(f_t)\|_*^2 \geq 2\lambda[R(f_t) - R(f^*)]. \quad (54)$$

We apply the above property to  $\Gamma_t$  [cf. (41)], i.e., the left-hand side of the above expression, to simplify (53) as follows:

$$\mathbb{E}[R(f_{t+1}) - R(f^*)] \leq (1 - \rho)\mathbb{E}[R(f_t) - R(f^*)] + L_1\eta^2\sigma^2 + \left(\frac{\eta\omega_1}{2} + L_1\eta^2\right)\alpha^2 \quad (55)$$

where constant  $\rho = 2\lambda\left(D\eta - \frac{\eta}{2\omega_1} - DL_1c^2\eta^2\right)$  determines the transient rate of convergence. Next, we solve for conditions on constants  $D$  and  $\omega_1$  such that the following holds:

$$0 \leq \rho \leq 1 \quad (56)$$

Define constants  $q_1 = 2\lambda \left(D - \frac{1}{2\omega_1}\right)$  and  $q_2 = 2\lambda D L_1 c^2$  and note  $\rho = q_1 \eta - q_2 \eta^2$ . The constant  $q_1$  is required to be nonnegative to satisfy the aforementioned condition on  $\rho$ . Imposing this constraint then implies that the Peter Paul inequality constant  $\omega_1$  in (50) satisfies  $\omega_1 > \frac{1}{2D}$ , where  $D$  is the correlation constant in 37. These conditions together imply

$$\eta < \frac{1}{q_1 \left(1 - \frac{q_2}{q_1} \eta\right)} \quad (57)$$

Now if  $\rho \leq 1$ , and if  $\left(1 - \frac{q_2}{q_1} \eta\right) \leq 1$ , then  $\eta < \frac{1}{q_1}$  implies (57) holds. On the contrary,  $\rho \geq 0$  implies  $\eta < \frac{q_1}{q_2}$ . Overall, then, we obtain the valid step-size range as  $\eta < \min\left(\frac{1}{q_1}, \frac{q_1}{q_2}\right)$ .

So now going back to (55) and breaking down iteratively the right hand side of that equation along with considering the fact that  $\sum_{i=0}^t (1-\rho)^i \leq \sum_{i=0}^{\infty} (1-\rho)^i = \frac{1}{\rho}$ , we get

$$\mathbb{E}[R(f_{t+1}) - R(f^*)] \leq (1-\rho)^t \mathbb{E}[R(f_0) - R(f^*)] + \frac{1}{\rho} \left[ L_1 \eta^2 \sigma^2 + \left(\frac{\eta \omega_1}{2} + L_1 \eta^2\right) \alpha^2 \right] \quad (58)$$

as stated in (46). To obtain the result for the function iterates, apply strong convexity of  $R(\cdot)$  as in Assumption 3 to write  $\mathbb{E}[\|f_{t+1} - f^*\|^2] \leq \frac{2}{\lambda} \mathbb{E}[R(f_{t+1}) - R(f^*)]$ . Substituting this relation into (58) allows us to conclude (47). ■

**When the pseudo-gradient is a stochastic gradients.** Stochastic gradients are special case of pseudo-gradients which are available whenever the instantaneous cost is evaluable in closed form as in, for instance, kernel logistic regression [cf. (31)]. Note that stochastic gradients satisfy the stochasticity rule, i.e.  $\mathbb{E}[g_t | \mathcal{F}_t] = \nabla R(f_t)$ . To prove the almost sure convergence of RKHS-valued stochastic mirror descent with projections, only Assumption 2 and the next three conditions are required.

**Assumption 6.** *The function  $R_\psi(\cdot)$  is  $\lambda_1$ -strongly convex.*

**Assumption 7.** *The function  $\psi$  is 1-strongly convex.*

**Assumption 8.** *The projected stochastic gradient has bounded second moment given the filtration  $\mathcal{F}_t = \sigma(\{\mathbf{x}_i\}_{i=1}^{t-1})$ .*

$$\mathbb{E}[\|\hat{g}_t\|_*^2 | \mathcal{F}_t] \leq G^2 \quad (59)$$

Assumption 7 is required to lower bound the norm difference between the auxiliary iterates from the optima, i.e.  $\|z_t - z^*\|_*$  by the the norm difference between the actual function iterates and the optima, i.e.  $\|f_t - f^*\|$ . Assumptions 6 and 8 are standard in the literature and is required to show the almost sure convergence theorem for the stochastic case.

**Theorem 2.** Under Assumption 2 and Assumptions 6-8, upon running Algorithm 1 with constant step-size  $\eta$  and constant compression budget  $\epsilon$ , the iterates  $f_t$  converges almost surely to a neighbourhood in limit infimum as  $t \rightarrow \infty$ .

$$\liminf_{t \rightarrow \infty} \|f_t - f^*\| \leq \xi := \frac{\epsilon + \sqrt{\epsilon^2 + \eta^3 \lambda_1 G^2}}{2\eta \lambda_1} \quad (60)$$

where  $G$  is defined in (59) as the bound on the conditional second-moment of the stochastic gradient in the dual norm and  $\lambda_1$  is the strong-convexity parameter.

*Proof of Theorem 2:* The proof starts by taking the dual Hilbert norm difference between  $z_{t+1}$  and  $z^* = \nabla \psi(f^*)$ , where  $z^*$  is taken to be the transformed function of the optimum  $f^*$  in the dual space, and then expanding  $z_{t+1}$  same as (40) as shown below

$$\|z_{t+1} - z^*\|_*^2 = \|z_t - \eta \hat{g}_t - z^*\|_*^2 \quad (61)$$

$$= \|z_t - z^*\|_*^2 - 2\eta \langle z_t - z^*, \hat{g}_t \rangle + \eta^2 \|\hat{g}_t\|_*^2 \quad (62)$$

$$= \|z_t - z^*\|_*^2 - 2\eta \langle z_t - z^*, g_t \rangle + 2\eta \langle z_t - z^*, g_t - \hat{g}_t \rangle + \eta^2 \|\hat{g}_t\|_*^2, \quad (63)$$

where the last equation is obtained by addition and subtraction of the actual stochastic gradient  $g_t$ . The third term on the right hand side of (63) can be upper bounded using Cauchy-Schwartz inequality and then application of (42) on it yields the bound

$$\|z_{t+1} - z^*\|_*^2 \leq \|z_t - z^*\|_*^2 - 2\eta \langle z_t - z^*, g_t \rangle + 2\epsilon \|z_t - z^*\|_* + \eta^2 \|\hat{g}_t\|_*^2. \quad (64)$$

So now taking conditional expectation given the past sigma algebra  $\mathcal{F}_t$  and using Assumption 8, we get

$$\mathbb{E}[\|z_{t+1} - z^*\|_*^2 | \mathcal{F}_t] \leq \|z_t - z^*\|_*^2 - 2\eta \langle z_t - z^*, \nabla R(f_t) \rangle + 2\epsilon \|z_t - z^*\|_* + \eta^2 G^2. \quad (65)$$

We assumed  $R_\psi(\cdot)$  to be the risk function which takes the auxiliary function  $z_t$  as an argument such that  $R_\psi(z_t) = R_\psi(\nabla\psi(f_t)) = R(f_t)$ , where  $R(\cdot)$  is our actual risk function. Hence, using this property and convexity of  $R_\psi$  and then Assumption 6, the second term on the right hand side of (65) can be simplified as

$$\langle z_t - z^*, \nabla R(f_t) \rangle = \langle z_t - z^*, \nabla R_\psi(z_t) \rangle \quad (66)$$

$$\geq R_\psi(z_t) - R_\psi(z^*) \quad (67)$$

$$\geq \frac{\lambda_1}{2} \|z_t - z^*\|_*^2. \quad (68)$$

So now using (68) in (65), the inequality further simplifies to

$$\mathbb{E}[\|z_{t+1} - z^*\|_*^2 | \mathcal{F}_t] \leq (1 - \eta\lambda_1) \|z_t - z^*\|_*^2 + 2\epsilon \|z_t - z^*\|_* + \eta^2 G^2. \quad (69)$$

A stopping stochastic process can be constructed using inequality (69), that tracks when  $\|z_t - z^*\|_*^2$  reaches the sub-optimal threshold. When the threshold is achieved, the function converges to the neighbourhood of the optimum. In order to establish this fact, we construct a stochastic process  $\delta_t$  such that the supermartingale condition is satisfied, i.e.  $\mathbb{E}[\delta_{t+1} | \mathcal{F}_t] \leq \delta_t$ . We would like to find out the threshold from (69) by finding out the roots for  $\|z_t - z^*\|$  when the following holds true

$$\mathbb{E}[\|z_{t+1} - z^*\|_*^2 | \mathcal{F}_t] \leq \|z_t - z^*\|_*^2 \quad (70)$$

$$(1 - \eta\lambda_1) \|z_t - z^*\|_*^2 + 2\epsilon \|z_t - z^*\|_* + \eta^2 G^2 \leq \|z_t - z^*\|_*^2. \quad (71)$$

(71) simplifies to the following quadratic inequality

$$-\eta\lambda_1 \|z_t - z^*\|_*^2 + 2\epsilon \|z_t - z^*\|_* + \eta^2 G^2 \leq 0. \quad (72)$$

The roots of the polynomial are

$$\|z_t - z^*\|_* = \frac{-2\epsilon \pm \sqrt{4\epsilon^2 + 4(\eta\lambda_1)(\eta^2 G^2)}}{-4\eta\lambda_1} \quad (73)$$

$$= \frac{\epsilon \mp \sqrt{\epsilon^2 + \eta^3 \lambda_1 G^2}}{2\eta\lambda_1}. \quad (74)$$

The inequality (72) opens downwards and since  $\|z_t - z^*\|_*$  is always positive, hence only positive root will be taken. So the radius of the convergence can be represented as

$$\xi := \frac{\epsilon + \sqrt{\epsilon^2 + \eta^3 \lambda_1 G^2}}{2\eta\lambda_1}. \quad (75)$$

So using (75), let's now define the stopping stochastic process  $\delta_t$  as

$$\delta_t = \|z_t - z^*\|_* \mathbb{I} \left\{ \min_{u \leq t} -\eta\lambda_1 \|z_u - z^*\|_*^2 + 2\epsilon \|z_u - z^*\|_* + \eta^2 G^2 > \xi \right\}, \quad (76)$$

where  $\mathbb{I}$  denotes the indicator function. Note  $\delta_t \geq 0$  since both the norm and the indicator are non-negative. So when the indicator condition  $\min_{u \leq t} -\eta\lambda_1 \|z_u - z^*\|_*^2 + 2\epsilon \|z_u - z^*\|_* + \eta^2 G^2 > \xi$  is satisfied, we may compute the square root of (70) yielding

$$\mathbb{E}[\delta_{t+1} | \mathcal{F}_t] \leq \delta_t. \quad (77)$$

Now taking the contrary condition, i.e.,  $\min_{u \leq t} -\eta\lambda_1 \|z_u - z^*\|_*^2 + 2\epsilon \|z_u - z^*\|_* + \eta^2 G^2 \leq \xi$ , makes the indicator to be 0 for the subsequent iterates, since min is used inside the indicator. So, in either case, (77) holds, which implies that  $\delta_t \xrightarrow{a.s.} 0$  as  $t \rightarrow \infty$ . This further implies the fact that either  $\lim_{t \rightarrow \infty} \|z_t - z^*\|_* - \xi = 0$  or the indicator goes to null for large  $t$  almost surely, i.e.  $\lim_{t \rightarrow \infty} \mathbb{I} \left\{ \min_{u \leq t} -\eta\lambda_1 \|z_u - z^*\|_*^2 + 2\epsilon \|z_u - z^*\|_* + \eta^2 G^2 > \xi \right\} = 0$ . Hence any of these conditions terminating to null translates to our convergence in the neighbourhood

$$\liminf_{t \rightarrow \infty} \|z_t - z^*\|_* \leq \xi. \quad (78)$$

Now using 7, we can write

$$\|z_t - z^*\|_* = \|\nabla\psi(f_t) - \nabla\psi(f^*)\|_* \geq \|f_t - f^*\|. \quad (79)$$

Using (79) in (78) concludes the proof of theorem 2. ■

Note that the almost sure convergence established for stochastic gradients in theorem 2 is a much stronger bound than that of the pseudo-gradient convergence result given in theorem 1. Hence when stochastic gradient computation is feasible, as in Kernel logistic regression for multi-class classification, on running SPPOT we can almost surely reach to the neighborhood of the optima.

**Parameterization efficiency.** We analyze the complexity of the function parameterization associated with Algorithm 1 when employing sparse projections defined by KOMP. To do so, we require additional two conditions.

**Assumption 9.** The pseudo-gradient may be written in the form  $g_t = g'_t \kappa(\mathbf{x}_t, \cdot)$  with scalar  $g'_t$  bounded by constant  $C$

$$|g'_t| \leq C \quad (80)$$

**Assumption 10.** The feature space  $\mathcal{X}$  is compact.

Assumption 9 implies that either the objective is differentiable or there exists a suitable kernel embedding such that the chain rule is applicable. Moreover, Assumption 10 ensures that the data domain has finite covering number [16]. Under these conditions, we establish that the model order of the function parameterization defined by Algorithm 1 is finite via analogous logic to [34][Theorem 4], stated here as a corollary.

**Corollary 3.** Denote as  $M_t$  the model order of the function  $z_t$  obtained from running Algorithm 1 with fixed compression budget  $\epsilon > 0$ . Then we have that  $M_t \leq M^\infty$ , where  $M^\infty$  is the maximum model order upper-estimated as

$$M^\infty \leq \mathcal{O}\left(\frac{1}{\epsilon}\right)^d \quad (81)$$

*Proof:* Begin by recalling the definition of the function approximation error of KOMP (Algorithm 2)

$$\gamma_j := \left\| \tilde{z} - \sum_{\mathbf{x}_n \in \mathcal{D} \setminus \{\mathbf{x}_j\}} w_n \kappa(\mathbf{x}_n, \cdot) \right\|_*$$

used to determine the compression stopping criteria.  $M_t$  is the model order of  $z_t$  and the model order of  $\tilde{z}_{t+1}$  is  $M_t + 1$  for addition of single data point. The expression for  $\gamma_{M_t+1}$  then is given as

$$\gamma_{M_t+1} = \left\| \tilde{z}_{t+1} - \sum_{\mathbf{x}_n \in \mathcal{D}_{t+1} \setminus \{\mathbf{x}_{M_t+1}\}} w_n \kappa(\mathbf{x}_n, \cdot) \right\|_* \quad (82)$$

Substitute in the definition  $\tilde{z}_{t+1} = z_t - \eta g_t$ , and note that dictionary elements are deleted if

$$\min_{j=1, \dots, M_t+1} \gamma_j \leq \epsilon. \quad (83)$$

We note that  $\gamma_j$  for  $j = 1, \dots, M_t+1$  is lower-bounded by  $\gamma_{M_t+1}$ , so it suffices to consider  $\gamma_{M_t+1}$ . Since the pseudo-gradient is assumed differentiable, i.e.  $g_t = g'_t \kappa(\mathbf{x}_t, \cdot)$  (Assumption 9), one may reduce this condition to the set distance between the dual of the subspace defined by the current dictionary and the kernel evaluated at the latest sample  $\mathbf{x}_t$  by applying similar logic to [34, Appendix D.1 Eq. (70)-(75) and Lemma 10], that is, the following holds

$$\text{dist}(\kappa(\mathbf{x}_t, \cdot), \mathcal{H}_{\mathcal{D}_t}^*) \leq \frac{\epsilon}{\eta |g'_t|} = \frac{\alpha}{|g'_t|} \quad (84)$$

There are two possibilities: either a new point is added or it is not. If it is not, then  $M_{t+1} \leq M_t + 1$  and the model order does not change. Let's consider when this condition is violated, such that the model order increases, i.e.,  $M_{t+1} = M_t + 1$ :

$$\text{dist}(\kappa(\mathbf{x}_t, \cdot), \mathcal{H}_{\mathcal{D}_t}^*) > \frac{\epsilon}{\eta |g'_t|} = \frac{\alpha}{|g'_t|} \quad (85)$$

Assumption 9 implies  $\frac{1}{|g'_t|} \geq \frac{1}{C}$ , which allows us to rewrite the preceding expression as

$$\text{dist}(\kappa(\mathbf{x}_t, \cdot), \mathcal{H}_{\mathcal{D}_t}^*) > \frac{\epsilon}{\eta C} = \frac{\alpha}{C} \quad (86)$$

KOMP stopping criteria is violated when distinct dictionary points  $\mathbf{d}_n$  and  $\mathbf{d}_j$  for  $j, n \in \{1, \dots, M_t\}$  satisfy the condition  $\|\phi(\mathbf{d}_n) - \phi(\mathbf{d}_j)\|_* > \frac{\epsilon}{\eta C} = \frac{\alpha}{C}$ . By Assumption 10, the number of Euclidean balls of radius  $\frac{\epsilon}{\eta C}$  required to cover the feature kernelized space  $\phi(\mathbf{x}) = \kappa(\mathbf{x}, \cdot)$  is always finite by the continuity of the kernel. Therefore, there exists a finite  $t$  such that (84) holds which implies that equation (83) is always valid, meaning the model order does not grow. More specifically, there exists a finite maximum model order  $M^\infty < \infty$  such that  $M_t < M^\infty$ , holds for all  $t$ .

Now if the kernel taken is Lipschitz continuous on the set  $\mathcal{X}$  which is compact by Assumption 10, then similar to [51, Proposition 2.2], the maximum model order  $M^\infty$  is bounded as (81), which yields an upper-bound on  $M^\infty$  for all  $t$ . ■

In the following section, we experiment with the aforementioned accuracy/complexity tradeoffs characterized presented.

## V. EXPERIMENTS

We shift to experimental validation of Algorithm 1 as compared with state of the art offline and online benchmarks for intensity function estimation in inhomogeneous Poisson Point Processes (PPP) and Kernel multi-class logistic regression over MNIST data set. Throughout, we select as our pseudo-gradient either kernel embedding or stochastic gradient – see Sec. III.

For compression algorithm aka KOMP to be used in the SPPPOT algorithm, we employ both constant and adaptive budgeting techniques. Constant budget is the same as described in [34], i.e.  $\epsilon$  is constant throughout the experiment. The major drawback of constant budgeting is the fact that some trial and error needs to be done for selecting the constant budget to obtain a reasonable model order, which may be eliminated with adapting the budget selection according to the model order of the current dictionary. Remember that  $\epsilon = \alpha\eta$ . Since the step size  $\eta$  is constant, the adaptation has been done by adapting  $\alpha$  (before the addition of data points in each iteration) according to the formula:

$$\alpha(t+1) = \alpha(t) \left[ 1 + \max \left( \min \left( (M_t - d_{mo}) \times 0.1\%, 0.1 \right), -0.1 \right) \right]$$

where  $\alpha(t+1)$  has an enforced upper and lower bound to ensure it remains nonzero even when near the target dictionary size  $d_{mo}$ . The intuition is that this constant increases when the model order  $M_t$  starts increasing from  $d_{mo}$  so that we allow a bit higher error tolerance budget  $\epsilon_{t+1} = \alpha(t+1)\eta$ , that results in reduction of  $M_{t+1}$ . The contrary is true when  $M_t < d_{mo}$ .

### A. Poisson point process normalized intensity estimation

For PPP pdf estimation (Example 1) of function  $f$ , the negative log-likelihood (27) (identical to [42, Eq. (3.1)]) defines the loss, whose minimization over time may be executed via Algorithm 1. Details about initialization and parametric updates are in Sec. III-1. For comparison, batch offline MLE BFGS (quasi-Newton) minimization method [42] and also Pseudo Mirror Descent (PMD) [38] are implemented. BFGS is included in 'fminunc' package of MATLAB with intensity given by  $f(\cdot) = af'(\cdot)^2$  where  $a$  is a positive scalar used for tuning and  $f'(\cdot)$  is the RKHS function.  $f(\cdot)$  is the actual intensity function expressed via  $f'(\cdot)^2$  to preserve positivity.

PMD is implemented using the [38, Eq. (8)] and the pseudo gradient  $g_t$  given in [38, section 3.1] constructed via kernel embedding. The PMD algorithm is a pointwise learning process where the function amplitude is learnt at specific uniform grid points. PMD has no concept of dictionary, and instead employs a fixed collection of uniform grid points  $u_j$  (see Sec. III-1), and fits an amplitude weight for each uniform grid point, but not at any Poisson samples. This precludes us from evaluating the loss at Poisson training/test samples. We further note that the PMD loss function [38, Eq. (8)] has the optimal intensity  $f^*$  term, which is unknown for the real world data. These subtleties motivate us to consider Root Mean Square Error (RMSE) and Integrated Square Error (ISE) as our performance metrics for benchmarking the comparators for synthetic data. For real world data, since evaluating these parameters are not possible, we will focus on the intensity function learnt for comparing PMD and can compare the offline BFGS and SPPPOT using the loss evaluation.

1) *Simulation for 1-D Gaussian toy example:* This is synthetic experiment illuminates the merits and drawbacks of SPPPOT relative to the alternatives. Our aim is to obtain the actual underlying PDF of the Point process. In the Gaussian toy example case, we prioritize three metrics: test set loss, RMSE and ISE. The metric ISE is defined as:

$$\text{ISE} = \int_{\mathcal{X}} (f(x) - f^*(x))^2 dx \quad (87)$$

where  $f(\cdot)$  is the estimated function and  $f^*(\cdot)$  is the underlying ground truth. This integral is evaluated numerically in our experiment. Since this is a synthetic experiment, we know the actual ground truth intensity function beforehand. Hence, metrics like RMSE and ISE can help us understand how well the function learnt is close to the ground truth. For synthetic 1-D Gaussian toy example, in addition to implementing SPPPOT algorithm with KL divergence as Bregman divergence, we also show the learning process of SPPPOT using squared RKHS-norm difference which is nothing but the simple FSGD updates with KOMP. This will illuminate the importance of selecting an appropriate Bregman divergence in Algorithm 1.

**Dataset.** For synthetic simulations, 10211 training data and 1001 test data is generated from a non-homogeneous PPP model having Gaussian pdf  $f(x) = \frac{10}{\sqrt{2\pi}} \exp(50(x - 0.5)^2)$ . All data points  $x \in (0, 1)$  are 1-D and have restricted range.

**Parameter selection.** For the purpose of experiments, throughout we select Gaussian kernel with bandwidth 0.0065 tuned to the standard deviation on a validation set 0.0806 via Silverman's rule of thumb [52]. For SPPPOT, we implement both the constant and adaptive parsimony constant. We run the offline BFGS scheme for only a single training epoch, as its compute time is about 6 hours. For SPPPOT, PMD and FSGD with KOMP, 8 training epochs of the experimental data are executed which run in about 5 minutes. We note that doing so ended up being required for PMD to converge reliably. The mini-batch size  $n = 30$  for SPPPOT (both constant and adaptive budget), PMD and also FSGD with KOMP so that loss is reduced and RMSE/ISE is minimized the most. The step size  $\eta$  is chosen by trial and error and is taken to be 0.012 for SPPPOT (both constant and adaptive budget), 0.05 for PMD and 0.006 for FSGD with KOMP. The number of uniform grid points  $u_j$ 's are taken to be 100 in 1-D Gaussian toy example distributed uniformly between 0 to 1. Since the weight amplitude of those 100

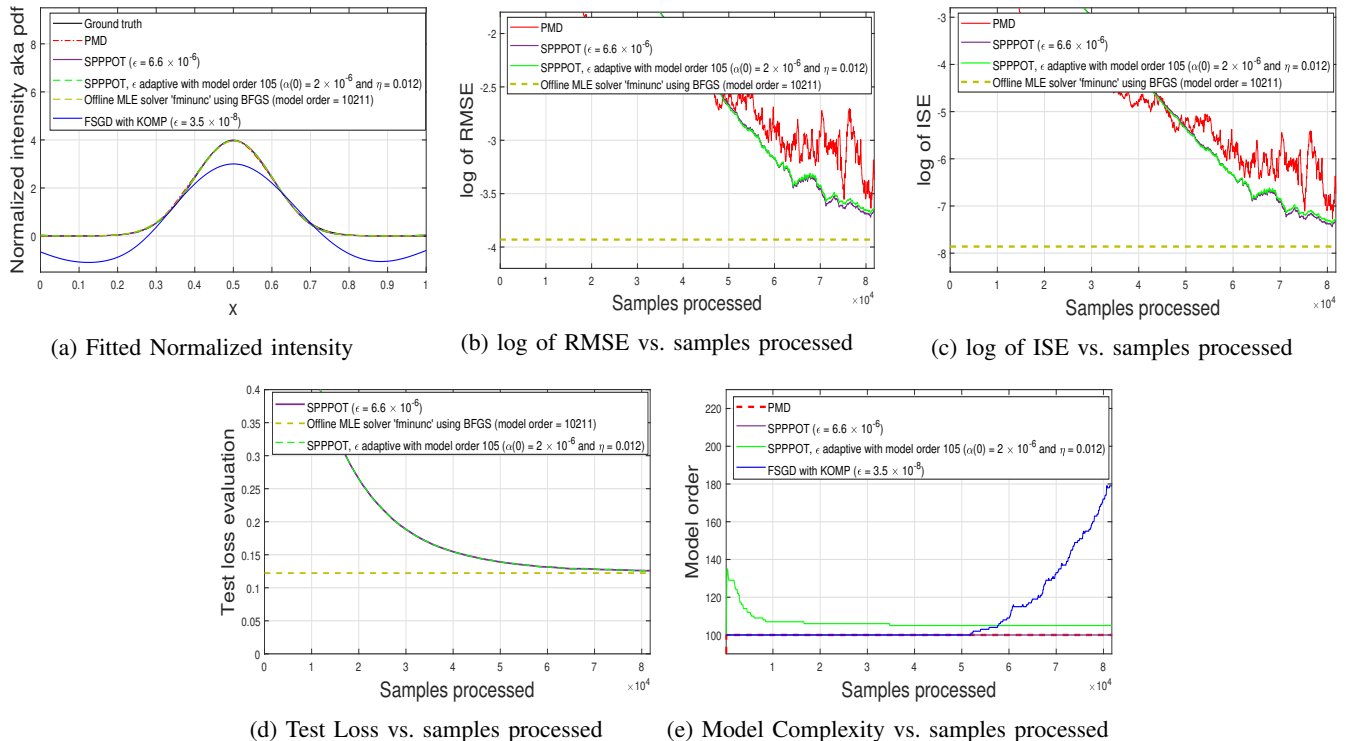


Fig. 1: We compare SPPPOT (Algorithm 1) (both constant and adaptive budgets) with PMD and offline BFGS algorithm on 1-D synthetic Gaussian toy example. FSGD with KOMP, known as POLK, is also implemented with constant budget to emphasize that it violates the range constraint. SPPPOT beats the state of the art online PMD algorithm with the same model order, and approaches performance of the offline solver. SPPPOT identifies how many statistically significant Poisson samples are required for convergence.

points are updated and kernel evaluation with respect to those 100 points are done in every iteration, hence model order for PMD is always 100. For SPPPOT with constant budget,  $\epsilon = 6.6 \times 10^{-6}$  is taken so that we can achieve model order of 100 in comparison to PMD. The SPPPOT algorithm can also be carried out by keeping Poisson points in addition to the uniform grid points in the dictionary. We have used SPPPOT with adaptive budget to demonstrate this fact. The desired model order  $d_{mo}$  is taken as 105 and the parameter  $\alpha(0) = 2 \times 10^{-6}$ . The KOMP budget is fixed at  $\epsilon = 3.5 \times 10^{-8}$  for FSGD with KOMP. For BFGS algorithm, the entire batch of training data is feed into the system and the function 'fminunc' takes care of the step size selection. BFGS uses a scaling factor  $a$  taken as 0.15 by cross validation of the loss over a validation set of 2000 points.

**Results.** The pdf obtained through different algorithms of the underlying 1-D Gaussian example is given in Fig. 1a. The corresponding model order, log of RMSE, log of ISE and the test loss evaluation with respect to the number of samples processed are given in Figs. 1e, 1b, 1c and 1d respectively. In Fig. 1a we observe that PMD, SPPPOT and BFGS yield densities near the ground truth, whereas FSGD with KOMP does not since it yields infeasible points, i.e., it yields density estimates that become negative at a few places. Moreover, the associated test loss, test RMSE and test ISE for this algorithm are 2.0148, 5.8317, and 34.0425, respectively, which is relatively high compared to the others that employ Bregman divergence/offline solvers. This underscores the importance of using the I-Divergence in Algorithm 1 to preserve positivity.

Observe that in Fig. 1b and Fig. 1c, SPPPOT with constant budget outperforms PMD for the same model order. Moreover, the noisy evolution of of RMSE and ISE for PMD is due to the large step-size required for hand-tuning optimal step-size choice. Reducing the step-size results in a larger gap between PMD and SPPPOT. SPPPOT with adaptive budget is also shown with desired model order 105 which also beats the PMD algorithm. The performance of SPPPOT constant budget (model order 100) and SPPPOT adaptive budget (model order 105) are comparable.

The function learnt by all the online algorithms will yield the normalized intensity. But for BFGS, the function learnt is the total intensity and is normalized by the number of training data and the pdf is plotted in Fig. 1a. The model order for BFGS algorithm is always 10211, which is omitted from Fig. 1e due to scale issues. 'fminunc' package for BFGS returns the function learnt after the completion of total learning process. Hence RMSE, ISE and test loss can be evaluated at the final function iterate and is presented in the corresponding figures as a dotted line. Fig. 1d demonstrates the fact that the converged test loss for our algorithm SPPPOT is quite close to the benchmark of BFGS.

Regarding offline vs. online compute time: SPPPOT, PMD and FSGD with KOMP took about 5 minutes to complete 8

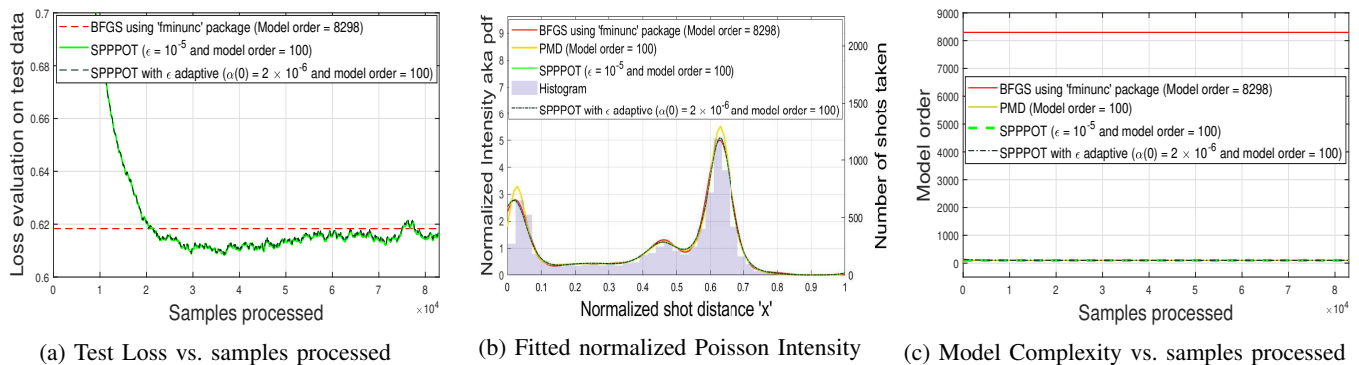


Fig. 2: We compare a BFGS solver for an offline MLE problem [42] as well as existing incremental techniques which do not incorporate complexity-reducing projections, i.e., stochastic Pseudo-mirror descent (PMD) [38] on the NBA dataset of Stephen Curry. SPPPOT yields a state of the art accuracy and complexity tradeoff for quickly fitting the intensity parameter of this inhomogeneous Poisson Process.

epochs, whereas BFGS takes about 6 hours for a single epoch. Hence considering all the aspects stated above, SPPPOT with KL divergence yields a favorable accuracy/complexity tradeoff.

Regarding the implementation of mini-batching, we note that the stochastic gradient belongs to the probability simplex, but a sum of stochastic gradients does not. To demonstrate this fact, one can take the same example of mini-batching but without gradient averaging. If the mini-batch size is  $m$ , then the function learnt has to be multiplied with  $\frac{N}{m}$  to get the intensity function. Therefore, normalization by the mini-batch size is required to remove ambiguity with respect to the normalization of the intensity estimate. Doing so then ensures that the RKHS element integrates to unity at each time. In addition, the normalization of the accumulated gradients for mini-batching will reduce the error, as we are taking the convex combination of the gradients. Taking this factor into consideration, we aim to learn the pdf.

2) *Experiments with Stephen Curry data:* We now shift to validating SPPPOT for estimating the normalized intensity function  $f(\cdot)$  on the NBA dataset of Stephen Curry which has shot distances as data samples  $x \in \mathbb{R}$ . Shot distances less than 40 are taken and the data is normalized. For this experiment also, we compare SPPPOT with online PMD and offline benchmark BFGS.

**Parameter Selection** We split data into 8298 training examples and 1000 test samples. BFGS is ran on a single epoch of the data, where as 10 epochs are being run for PMD and SPPPOT (both constant and adaptive budgeting). For the purpose of experiments, Gaussian kernel is taken with kernel bandwidth 0.0025. The constant  $a$  for BFGS is taken to be 1 by cross validation over randomly selected 1000 points from the train data. The mini-batch size is taken to be 30 for both SPPPOT and PMD. The step size  $\eta$  are taken to be 0.03 and 0.1 for SPPPOT and PMD respectively by trial and error. The KOMP budget for SPPPOT constant budgeting is fixed at  $\epsilon = 10^{-5}$  so that model order matches with the number of uniform grid points for PMD. For SPPPOT with adaptive budgeting, we set  $d_{mo} = 100$  and  $\alpha(0) = 2 \times 10^{-6}$ . Note that the 100 points kept in the dictionary for SPPPOT are the 100 uniform grid points only. If required one can opt for a higher model order by reducing the budget where some Poisson points will also be kept.

**Results** The training loss, the estimated probability density function (pdf), i.e., intensity, and the model order are given in Figs. 2a, 2b, and 2c, respectively. Observe that the stochastic gradient belongs to the probability simplex due to gradient averaging. Hence the function learnt using PMD and SPPPOT preserve feasibility, whereas the one obtained using BFGS has to be normalized with the number of training data points to obtain a density. Moreover, BFGS took about 5 hours to compute, as compared with online approaches: PMD and SPPPOT finished 10 epochs in about 7 minutes. This runtime difference is reflected in the model complexity difference in 2c. Moreover, SPPPOT outperforms the batch solver after a few training epochs (Fig. 2a), and yields a pdf much closer to the offline baseline BFGS compared to the previous online approach PMD that does not incorporate sparse projections for point selection.

### B. Kernel multi-class logistic regression

Next we consider the problem of Kernel Logistic Regression (KLR) (Example 2, whose loss is (5) and stochastic gradient takes the form (31). For SPPPOT, we have taken KL divergence as the Bregman divergence and considered both constant and adaptive parsimony constants. We have compared SPPPOT with the online algorithm POLK [34] (without the regularizer term) and with the offline batch algorithm Functional Gradient Descent (FGD) without any dictionary compression. We ran FGD for 1000 iterations. We have also compared with the multi-class kernel SVM (KSVM) solver in LIBSVM package [53], which is also a batch algorithm. Even though it uses the KSVM algorithm, not KLR and the loss function is also different, still it is a



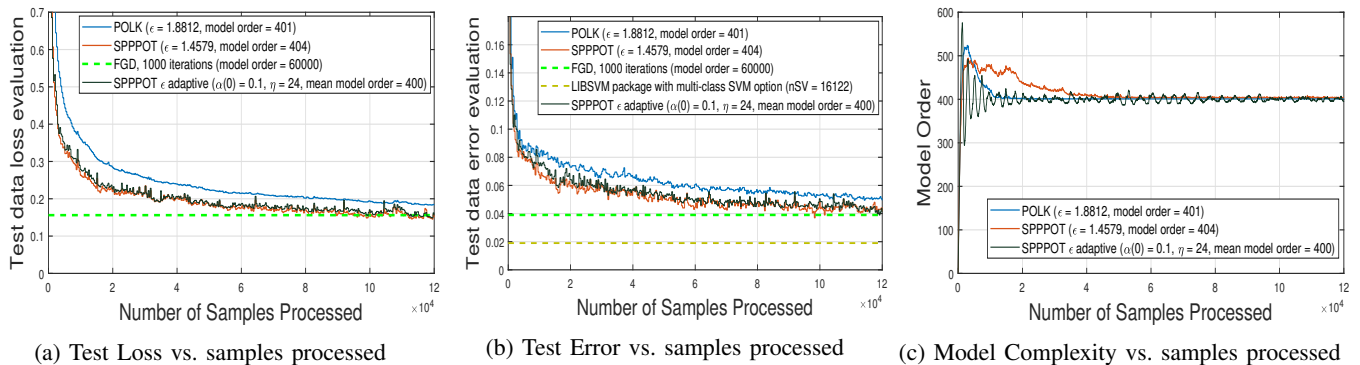


Fig. 3: We compared SPPPOT algorithm (both constant and adaptive budgets) with POLK [34] and offline FGD over MNIST dataset for solving KLR. SPPPOT obtains competitive accuracy with LIBSVM package, although it is computable online.

classification algorithm and is used as a baseline to plot the classification error at the end which is shown as a dotted baseline in Fig. 3b.

**Dataset:** We consider algorithm performance for the problem of classifying MNIST handwritten digits [41], which consists of 60000 data points for training and 10000 data points for testing. Out of 10000 training points, we randomly sampled 2000 points for our training purpose. Each data point is an image of a handwritten digit, and the goal is to label each images into the corresponding digit. We simply read the images into a 784-dimensional feature vector and scaled the pixel values ranging from 0 to 255 to the intensities in  $[0, 1]$ .

**Parameter selection:** We select the Gaussian kernel with bandwidth selected by cross-validation over 3.33% of the training data (randomly chosen 2000 points) and the KOMP budget is kept as zero during cross-validation for both POLK and SPPPOT, which yielded bandwidth is taken as 16 (standard deviation 4) for all experiments. A single epoch of training data is fed to both FGD and LIBSVM (C-SVC option) whereas 2 epochs are being run for the online algorithms POLK and SPPPOT (both constant and adaptive budget). The constant learning rate is taken by trial and error to be 24 for FGD, POLK and SPPPOT for both budget combinations. The KOMP budget is taken as  $\epsilon = 1.4579$  for SPPPOT with constant budget and  $\epsilon = 1.8812$  for POLK, which yield converged model orders, respectively, of 401 and 404. Matching the model orders for both the experiments is hard and here adaptive budgeting becomes handy. For SPPPOT with adaptive budget, we selected the desired model order as 400 and the constant  $\alpha(0) = 0.1$ . It is seen in Fig. 3c that the mean model order is 400 and the model order fluctuations with respect to the samples processed are all bounded and eventually converge. The storage requirement is finite and comparable to POLK with model order 401.

**Results:** The test loss, error and the model order plots with respect to samples processed has been presented in Figs. 3a, 3b and 3c respectively. Observe that SPPPOT with both constant and adaptive budgets outperforms POLK and obtains performance competitive with the offline benchmarks FGD and LIBSVM (C-SVC) whose parameterization complexity is 60000 and 16122, respectively, which are not depicted in the same figure due to scale. SPPPOT, after the loss and error settles down, performs comparably to FGD with 1000 iterates, whereas for POLK, there is still a considerable gap. FGD took about 12 hours to compute a single epoch with 1000 iterations. As seen in Fig. 3b, KVSVM has better accuracy than the asymptotic performance of KLR algorithms. Still we can say the test error for SPPPOT is within 2% of the LIBSVM solver and yields a more efficient parameterization.

## VI. CONCLUSION

We studied strongly convex expected risk minimization problems when the decision variable belongs to a Reproducing Kernel Hilbert Space (RKHS) and its target domain is required to be nonnegative, motivated by the intensity estimation of inhomogeneous point processes and supervised learning whose losses are associated with negative log-likelihoods. We put forth a variant of stochastic mirror descent that employs (i) *pseudo-gradients* and (ii) projections. Compressive projections are executed via KOMP, which mitigate complexity issues of RKHS parameterizations. We established accuracy/complexity tradeoffs between convergence in mean and bounds on the model complexity of the learned functions under standard assumptions. Experiments demonstrated competitive performance with the state of the art for inhomogeneous Poisson Process intensity estimation on synthetic data and for kernel logistic regression on real data. Future directions include scaling the intensity estimation approach to higher dimensions through convolutional kernels, as well as the use of event-triggers and censoring techniques for communication-efficient networking/actuation mechanisms.

## REFERENCES

- [1] Z. Marinho, B. Boots, A. Dragan, A. Byravan, G. J. Gordon, and S. Srinivasa, “Functional gradient motion planning in reproducing kernel hilbert spaces,” in *Proceedings of Robotics: Science and Systems*, AnnArbor, Michigan, June 2016.

- [2] G. Francis, L. Ott, and F. Ramos, "Stochastic functional gradient for motion planning in continuous occupancy maps," in *2017 IEEE International Conference on Robotics and Automation (ICRA)*. IEEE, 2017, pp. 3778–3785.
- [3] L. C. Drazek, "Intensity estimation for poisson processes," *The University of Leeds, School of Mathematics*, 2013.
- [4] K. P. Murphy, *Machine learning: a probabilistic perspective*. MIT press, 2012.
- [5] A. Berlinet and C. Thomas-Agnan, *Reproducing kernel Hilbert spaces in probability and statistics*. Springer Science & Business Media, 2011.
- [6] H. Ramlau-Hansen, "Smoothing counting process intensities by means of kernel functions," *The Annals of Statistics*, pp. 453–466, 1983.
- [7] J. Zhu and T. Hastie, "Kernel logistic regression and the import vector machine," in *Advances in neural information processing systems*, 2002, pp. 1081–1088.
- [8] S. Boyd, S. P. Boyd, and L. Vandenberghe, *Convex optimization*. Cambridge university press, 2004.
- [9] E. Dall'Anese, A. Simonetto, S. Becker, and L. Madden, "Optimization and learning with information streams: Time-varying algorithms and applications," *IEEE Signal Processing Magazine*, vol. 37, no. 3, pp. 71–83, 2020.
- [10] K. Slavakis, G. B. Giannakis, and G. Mateos, "Modeling and optimization for big data analytics:(statistical) learning tools for our era of data deluge," *IEEE Signal Processing Magazine*, vol. 31, no. 5, pp. 18–31, 2014.
- [11] A. Shapiro, D. Dentcheva, and A. Ruszczyński, *Lectures on stochastic programming: modeling and theory*. SIAM, 2014.
- [12] R. T. Rockafellar and R. J.-B. Wets, *Variational analysis*. Springer Science & Business Media, 2009, vol. 317.
- [13] T. T. Doan, S. Bose, D. H. Nguyen, and C. L. Beck, "Convergence of the iterates in mirror descent methods," *IEEE control systems letters*, vol. 3, no. 1, pp. 114–119, 2018.
- [14] A. Beck and M. Teboulle, "Mirror descent and nonlinear projected subgradient methods for convex optimization," *Operations Research Letters*, vol. 31, no. 3, pp. 167–175, 2003.
- [15] V. Kůrková, "Kolmogorov's theorem and multilayer neural networks," *Neural networks*, vol. 5, no. 3, pp. 501–506, 1992.
- [16] M. Anthony and P. L. Bartlett, *Neural network learning: Theoretical foundations*. cambridge university press, 2009.
- [17] T. Hofmann, B. Schölkopf, and A. J. Smola, "Kernel methods in machine learning," *The annals of statistics*, pp. 1171–1220, 2008.
- [18] A. Krizhevsky, I. Sutskever, and G. E. Hinton, "Imagenet classification with deep convolutional neural networks," in *Advances in neural information processing systems*, 2012, pp. 1097–1105.
- [19] D. Yu, G. Hinton, N. Morgan, J.-T. Chien, and S. Sagayama, "Introduction to the special section on deep learning for speech and language processing," *IEEE Transactions on Audio, Speech, and Language Processing*, vol. 20, no. 1, pp. 4–6, 2011.
- [20] Y. Goldberg, "A primer on neural network models for natural language processing," *Journal of Artificial Intelligence Research*, vol. 57, pp. 345–420, 2016.
- [21] N. Sünderrhauf, O. Brock, W. Scheirer, R. Hadsell, D. Fox, J. Leitner, B. Upcroft, P. Abbeel, W. Burgard, M. Milford *et al.*, "The limits and potentials of deep learning for robotics," *The International Journal of Robotics Research*, vol. 37, no. 4-5, pp. 405–420, 2018.
- [22] J. Mairal, "End-to-end kernel learning with supervised convolutional kernel networks," in *Advances in neural information processing systems*, 2016, pp. 1399–1407.
- [23] J. Kivinen, A. J. Smola, and R. C. Williamson, "Online learning with kernels," *IEEE transactions on signal processing*, vol. 52, no. 8, pp. 2165–2176, 2004.
- [24] Y. Lei and D.-X. Zhou, "Convergence of online mirror descent," *Applied and Computational Harmonic Analysis*, vol. 48, no. 1, pp. 343–373, 2020.
- [25] G. Kimeldorf and G. Wahba, "Some results on tchebycheffian spline functions," *Journal of mathematical analysis and applications*, vol. 33, no. 1, pp. 82–95, 1971.
- [26] C. K. Williams and M. Seeger, "Using the nystrom method to speed up kernel machines," in *Advances in neural information processing systems*, 2001, pp. 682–688.
- [27] C. Richard, J. Carlos, M. Bermudez, and P. Honeine, "Online prediction of time series data with kernels," *IEEE Trans. Signal Process.*, vol. 57, no. 3, pp. 1058–1067, 2009.
- [28] W. Liu, P. P. Pokharel, and J. C. Principe, "The kernel least-mean-square algorithm," *IEEE Trans. Signal Process.*, vol. 56, no. 2, pp. 543–554, 2008.
- [29] A. Rahimi and B. Recht, "Random features for large-scale kernel machines," in *Advances in neural information processing systems*, 2008, pp. 1177–1184.
- [30] Y. Yang, M. Pilanci, M. J. Wainwright *et al.*, "Randomized sketches for kernels: Fast and optimal nonparametric regression," *The Annals of Statistics*, vol. 45, no. 3, pp. 991–1023, 2017.
- [31] B. Dai, B. Xie, N. He, Y. Liang, A. Raj, M.-F. F. Balcan, and L. Song, "Scalable kernel methods via doubly stochastic gradients," in *Advances in Neural Information Processing Systems*, 2014, pp. 3041–3049.
- [32] Z. Wang, K. Crammer, and S. Vucetic, "Breaking the curse of kernelization: Budgeted stochastic gradient descent for large-scale svm training," *Journal of Machine Learning Research*, vol. 13, no. Oct, pp. 3103–3131, 2012.
- [33] S. G. Mallat and Z. Zhang, "Matching pursuits with time-frequency dictionaries," *IEEE Transactions on signal processing*, vol. 41, no. 12, pp. 3397–3415, 1993.
- [34] A. Koppel, G. Warnell, E. Stump, and A. Ribeiro, "Parsimonious online learning with kernels via sparse projections in function space," *Journal of Machine Learning Research*, vol. 20, no. 1, pp. 83–126, 2019.
- [35] A. Koppel, H. Pradhan, and K. Rajawat, "Consistent online gaussian process regression without the sample complexity bottleneck," *arXiv preprint arXiv:2004.11094*, 2020.
- [36] P. J. Diggle, P. Moraga, B. Rowlingson, B. M. Taylor *et al.*, "Spatial and spatio-temporal log-gaussian cox processes: extending the geostatistical paradigm," *Statistical Science*, vol. 28, no. 4, pp. 542–563, 2013.
- [37] I. Csiszár, "I-divergence geometry of probability distributions and minimization problems," *The annals of probability*, pp. 146–158, 1975.
- [38] Y. Yang, H. Wang, N. Kiyavash, and N. He, "Learning positive functions with pseudo mirror descent," in *Advances in Neural Information Processing Systems*, 2019, pp. 14 144–14 154.
- [39] J. Mairal, P. Koniusz, Z. Harchaoui, and C. Schmid, "Convolutional kernel networks," in *Advances in neural information processing systems*, 2014, pp. 2627–2635.
- [40] B. Poljak and Y. Z. Tsyppin, "Pseudogradient adaptation and training algorithms," *Automation and Remote Control*, vol. 34, pp. 45–67, 1973.
- [41] Y. LeCun, "The mnist database of handwritten digits," <http://yann.lecun.com/exdb/mnist/>.
- [42] S. Flaxman, Y. W. Teh, D. Sejdinovic *et al.*, "Poisson intensity estimation with reproducing kernels," *Electronic Journal of Statistics*, vol. 11, no. 2, pp. 5081–5104, 2017.
- [43] R. Wheeden and A. Zygmund, *Measure and Integral: An Introduction to Real Analysis*. Taylor and Francis, 1977.
- [44] V. Norkin and M. Keyzer, "On stochastic optimization and statistical learning in reproducing kernel hilbert spaces by support vector machines (svm)," *Informatica*, vol. 20, pp. 273–292, 2009.
- [45] A. Agarwal and J. C. Duchi, "Distributed delayed stochastic optimization," in *Advances in Neural Information Processing Systems*, 2011, pp. 873–881.
- [46] B. A. Frigyi, S. Srivastava, and M. R. Gupta, "Functional bregman divergence and bayesian estimation of distributions," *IEEE Trans. Inf. Theory*, vol. 54, no. 11, pp. 5130–5139, 2008.
- [47] C. Scovel, D. Hush, I. Steinwart, and J. Theiler, "Radial kernels and their reproducing kernel hilbert spaces," *Journal of Complexity*, vol. 26, no. 6, pp. 641–660, 2010.
- [48] P. Vincent and Y. Bengio, "Kernel matching pursuit," *Machine Learning*, vol. 48, pp. 165–187, 2002.
- [49] Y. Nesterov, "Primal-dual subgradient methods for convex problems," *Mathematical Programming*, vol. 120, pp. 221–259, 2009.

- [50] A. Nemirovski, A. Juditsky, G. Lan, and A. Shapiro, "Robust stochastic approximation approach to stochastic programming," *SIAM Journal on optimization*, vol. 19, no. 4, pp. 1574–1609, 2009.
- [51] Y. Engel, S. Mannor, and R. Meir, "The kernel recursive least-squares algorithm," *IEEE Transactions on signal processing*, vol. 52, no. 8, pp. 2275–2285, 2004.
- [52] B. W. Silverman, *Density estimation for statistics and data analysis*. CRC press, 1986, vol. 26.
- [53] C.-C. Chang and C.-J. Lin, "LIBSVM: A library for support vector machines," *ACM Transactions on Intelligent Systems and Technology*, vol. 2, pp. 27:1–27:27, 2011, software available at <http://www.csie.ntu.edu.tw/~cjlin/libsvm>.